The potassium channel subunit K_V1.8 (*Kcna10*) is essential for the distinctive outwardly rectifying conductances of type I and II vestibular hair cells

Hannah R Martin[1], Anna Lysakowski[2], Ruth Anne Eatock[1]*

[1]Department of Neurobiology, University of Chicago, Chicago, United States; [2]Department of Anatomy and Cell Biology, University of Illinois at Chicago, Chicago, United States

eLife assessment

This study provides direct evidence showing that K_V1.8 channels provide the basis for several potassium currents in the two types of sensory hair cells found in the mouse vestibular system. This is an **important** finding because the nature of the channels underpinning the unusual potassium conductance $g_{K,L}$ in type I hair cells has been under scrutiny for many years. The experimental evidence is **compelling** and the analysis is rigorous. The study will be of interest to cell and molecular biologists as well as vestibular and auditory neuroscientists.

*For correspondence:
eatock@uchicago.edu

Abstract

In amniotes, head motions and tilt are detected by two types of vestibular hair cells (HCs) with strikingly different morphology and physiology. Mature type I HCs express a large and very unusual potassium conductance, $g_{K,L}$, which activates negative to resting potential, confers very negative resting potentials and low input resistances, and enhances an unusual non-quantal transmission from type I cells onto their calyceal afferent terminals. Following clues pointing to K_V1.8 (*Kcna10*) in the Shaker K channel family as a candidate $g_{K,L}$ subunit, we compared whole-cell voltage-dependent currents from utricular HCs of K_V1.8-null mice and littermate controls. We found that K_V1.8 is necessary not just for $g_{K,L}$ but also for fast-inactivating and delayed rectifier currents in type II HCs, which activate positive to resting potential. The distinct properties of the three K_V1.8-dependent conductances may reflect different mixing with other K_V subunits that are reported to be differentially expressed in type I and II HCs. In K_V1.8-null HCs of both types, residual outwardly rectifying conductances include K_V7 (*Knq*) channels. Current clamp records show that in both HC types, K_V1.8-dependent conductances increase the speed and damping of voltage responses. Features that speed up vestibular receptor potentials and non-quantal afferent transmission may have helped stabilize locomotion as tetrapods moved from water to land.

Introduction

The receptor potentials of hair cells (HCs) are strongly shaped by large outwardly rectifying K⁺ conductances that are differentially expressed according to HC type. Here, we report that a specific voltage-gated K⁺ (K_V) channel subunit participates in very different K_V channels dominating the membrane conductances of type I and II HCs in amniote vestibular organs.

Type I HCs occur only in amniote vestibular organs. Their most distinctive features are that they are enveloped by a calyceal afferent terminal (*Wersall, 1956*; *Lysakowski and Goldberg, 2004*) and that

they express $g_{K,L}$ (*Correia and Lang, 1990*; *Rennie and Correia, 1994*; *Rüsch and Eatock, 1996a*): a large non-inactivating conductance with an activation range from –100 to –60 mV, far more negative than other 'low-voltage-activated' K_V channels. HCs are known for their large outwardly rectifying K^+ conductances, which repolarize membrane voltage following a mechanically evoked perturbation and in some cases contribute to sharp electrical tuning of the HC membrane. $g_{K,L}$ is unusually large and unusually negatively activated, and therefore strongly attenuates and speeds up the receptor potentials of type I HCs (*Correia et al., 1996*; *Rüsch and Eatock, 1996b*). In addition, $g_{K,L}$ augments non-quantal transmission from type I HC to afferent calyx by providing open channels for K^+ flow into the synaptic cleft (*Contini et al., 2012*; *Contini et al., 2017*; *Contini et al., 2020*; *Govindaraju et al., 2023*), increasing the speed and linearity of the transmitted signal (*Songer and Eatock, 2013*).

Type II HCs have compact afferent synaptic contacts (boutons) where the receptor potential drives quantal release of glutamate. They have fast-inactivating (A-type, g_A) and delayed rectifier (g_{DR}) conductances that are opened by depolarization above resting potential (V_{rest}).

The unusual properties of $g_{K,L}$ have long attracted curiosity about its molecular nature. $g_{K,L}$ has been proposed to include 'M-like' K_V channels in the K_V7 and/or erg channel families (*Kharkovets et al., 2000*; *Hurley et al., 2006*; *Holt et al., 2007*). The $K_V7.4$ subunit was of particular interest because it contributes to the low-voltage-activated conductance, $g_{K,n}$, in cochlear outer HCs, but was eventually eliminated as a $g_{K,L}$ subunit by experiments on $K_V7.4$-null mice (*Spitzmaul et al., 2013*).

Several observations suggested the $K_V1.8$ (KCNA10) subunit as an alternative candidate for $g_{K,L}$. $K_V1.8$ is highly expressed in vestibular sensory epithelia (*Carlisle et al., 2012*), particularly HCs (*Lee et al., 2013*; *Scheffer et al., 2015*; *McInturff et al., 2018*), with slight expression elsewhere (skeletal muscle, *Lee et al., 2013*; kidney, *Yao et al., 2002*). *Kcna10$^{-/-}$* mice show absent or delayed vestibular-evoked potentials, the synchronized activity of afferent nerve fibers sensitive to fast linear head motions (*Lee et al., 2013*). Unique among K_V1 channels, $K_V1.8$ has a cyclic nucleotide-binding domain (*Lang et al., 2000*) with the potential to explain $g_{K,L}$'s known cGMP dependence (*Behrend et al., 1997*; *Chen and Eatock, 2000*).

Our comparison of whole-cell currents and immunohistochemistry in type I HCs from *Kcna10$^{-/-}$* and *Kcna10$^{+/+,+/-}$* mouse utricles showed that $K_V1.8$ expression is necessary for $g_{K,L}$. More surprisingly, $K_V1.8$ expression is also required for A-type and delayed rectifier conductances of type II HCs. In both HC types, eliminating the $K_V1.8$-dependent major conductances revealed a smaller delayed rectifier conductance involving K_V7 channels. Thus, the distinctive outward rectifiers that produce such different receptor potentials in type I and II HCs both include $K_V1.8$ and K_V7 channels.

Results

We compared whole-cell voltage-activated K^+ currents in type I and II HCs from homozygous knockout (*Kcna10$^{-/-}$*) animals and their wildtype (*Kcna10$^{+/+}$*) or heterozygote (*Kcna10$^{+/-}$*) littermates. We immunolocalized $K_V1.8$ subunits in the utricular epithelium and pharmacologically characterized the residual K^+ currents of *Kcna10$^{-/-}$* animals. Current clamp experiments demonstrated the impact of $K_V1.8$-dependent currents on passive membrane properties.

We recorded from three utricular zones: lateral extrastriola (LES), striola, and medial extrastriola (MES); striolar and extrastriolar zones have many structural and functional differences and give rise to afferents with different physiology (reviewed in *Goldberg, 2000*; *Eatock and Songer, 2011*). Recordings are from 412 type I and II HCs (53% LES, 30% MES, 17% striola) from mice between postnatal day (P) 5 and P370. We recorded from such a wide age range to test for developmental or senescent changes in the impact of the null mutation. Above P18, we did not see substantial changes in K_V channel properties, as reported (*González-Garrido et al., 2021*).

Kcna10$^{-/-}$ animals appeared to be healthy and to develop and age normally, as reported (*Lee et al., 2013*), and HCs were healthy (see Methods for criteria).

$K_V1.8$ is necessary for $g_{K,L}$ in type I HCs

The large low-voltage-activated conductance, $g_{K,L}$, in *Kcna10$^{+/+,+/-}$* type I HCs produces distinctive whole-cell current responses to voltage steps, as highlighted by our standard type I voltage protocol (*Figure 1A*). From a holding potential within the $g_{K,L}$ activation range (here –74 mV), the cell is hyperpolarized to –124 mV, negative to E_K and the activation range, producing a large inward current
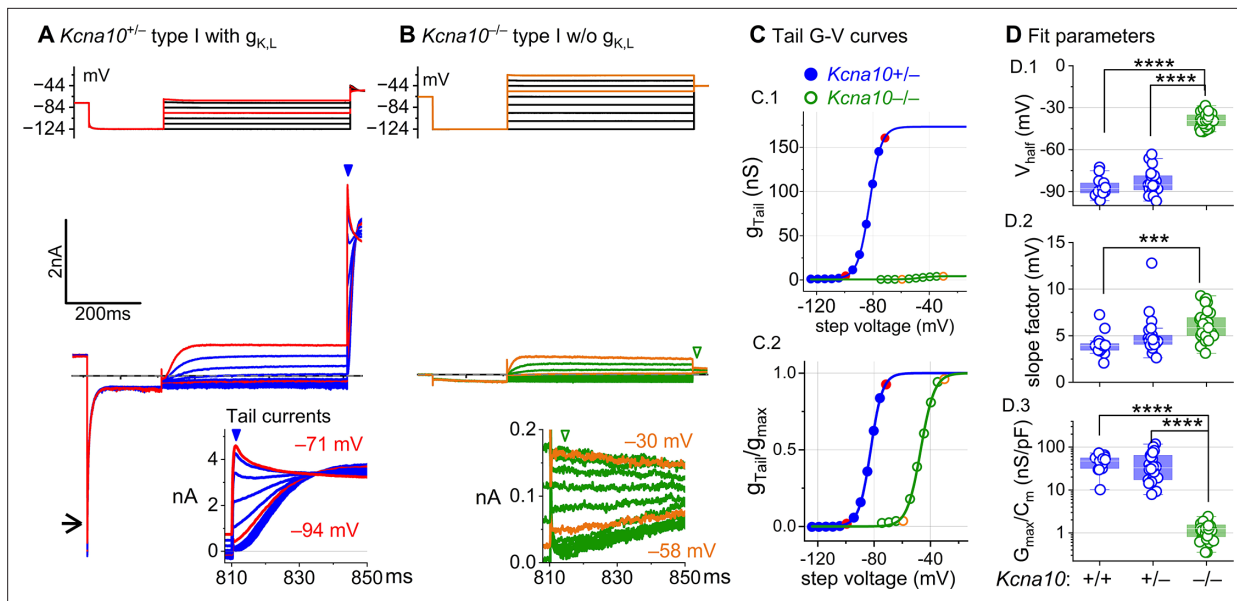
Figure 1. $Kcna10^{-/-}$ type I hair cells (HCs) lacked $g_{K,L}$, the dominant conductance in mature $Kcna10^{+/+,++/-}$ type I HCs. Representative voltage-evoked currents in (**A**) a P22 $Kcna10^{+/-}$ type I HC and (**B**) a P29 $Kcna10^{-/-}$ type I HC. (**A**) *Arrow,* transient inward current that is a hallmark of $g_{K,L}$. *Arrowheads,* tail currents, magnified in *insets.* For steps positive to the midpoint voltage, tail currents are very large. As a result, K^+ accumulation in the calyceal cleft reduces driving force on K^+, causing currents to decay rapidly, as seen in A (***Lim et al., 2011***). Note that the voltage protocol (top) in B extends to more positive voltages. (**C**) Activation (*G–V*) curves from tail currents in A and B; symbols, data; curves, Boltzmann fits (***Equation 1***). (**D**) Fit parameters from mice >P12 show big effect of $Kcna10^{-/-}$ and no difference between $Kcna10^{+/-}$ and $Kcna10^{+/+}$. (**D.1**), Tukey's test: +/+ vs –/–, p<1E-9; +/– vs –/–, p<1E-9. (**D.2**), Tukey's test: +/+ vs –/–, p=9.4E-4. (**D.3**), Tukey's test: +/+ vs –/–, p<1E-9; +/– vs –/–, p<1E-9. *Asterisks:* ***p < 0.001; and ****p < 0.0001. *Line,* median; *Box,* interquartile range; *Whiskers,* outliers. See ***Table 1*** for statistics.

The online version of this article includes the following figure supplement(s) for figure 1:

Figure supplement 1. Developmental changes in type I hair cell (HC) K_V conductances.

through open $g_{K,L}$ channels that rapidly decays as the channels deactivate. We use the large transient inward current as a hallmark of $g_{K,L}$. The hyperpolarization closes all $g_{K,L}$ channels, and then the activation function is probed with a series of depolarizing steps, obtaining the maximum conductance from the peak tail current at –44 mV (***Figure 1A***). We detected no difference between the Boltzmann parameters of $g_{K,L}$ *G–V* curves from $Kcna10^{+/-}$ and $Kcna10^{+/+}$ type I HCs.

For a similar voltage protocol, $Kcna10^{-/-}$ type I HCs (***Figure 1B***) produced no inward transient current at the step from holding potential to –124 mV and much smaller depolarization-activated currents during the iterated steps, even at much more positive potentials. ***Figure 1C*** compares the conductance–voltage (*G–V*, activation) curves fit to tail currents (***Equation 1***; see insets in ***Figure 1A, B***): the maximal conductance (g_{max}) of the $Kcna10^{-/-}$ HC was over 10-fold smaller (***Figure 1C.1***), and the curve was positively shifted by >40 mV (***Figure 1C.2***). ***Figure 1D*** shows the *G–V* Boltzmann fit parameters for type I HCs from mice >P12, an age at which type I HCs normally express $g_{K,L}$ (***Rüsch et al., 1998***).

In type I HCs from $Kcna10^{+/+,+,-}$ mice, the *G–V* parameters of outwardly rectifying currents transitioned over the first 15–20 postnatal days from values for a conventional delayed rectifier, activating positive to resting potential, to $g_{K,L}$ values (***Figure 1—figure supplement 1A***), as previously described (***Rüsch et al., 1998***; ***Géléoc et al., 2004***; ***Hurley et al., 2006***). Between P5 and P10, some type I HCs have not yet acquired the physiologically defined conductance, $g_{K,L}$. No effects of K_V1.8 deletion were seen in the delayed rectifier currents of immature type I HCs (***Figure 1—figure supplement 1B***), showing that they were not immature forms of the K_V1.8-dependent $g_{K,L}$ channels.

$Kcna10^{-/-}$ type I HCs had a much smaller residual delayed rectifier that activated positive to resting potential, with V_{half} ~–40 mV and g_{max} density of 1.3 nS/pF. No additional K^+ conductance activated up to +40 mV, and *G–V* parameters did not change much with age from P5 to P370. We characterize this K_V1.8-independent delayed rectifier later. A much larger non-$g_{K,L}$ delayed rectifier conductance ($g_{DR,I}$) was reported in our earlier publication on mouse utricular type I HCs (***Rüsch et al., 1998***). This current

Table 1. Type I hair cell K_V activation voltage dependence.
Mean ± SEM (number of cells). g is effect size, Hedge's g. KWA is Kruskal–Wallis ANOVA.

Zone	Kcna10	Tail $V_{1/2}$, mV*	Tail S, mV[†]	Tail g_{max}, nS[‡]	Tail g_{max}/C_m, nS/pF[§]	Age (median, range)
Extrastriola	+/+	−85 ± 2 (12)	4.3 ± 0.4 (12)	270 ± 40 (11)	47 ± 8 (11)	22, 14–287
	+/−	−83 ± 1 (40)	5.2 ± 0.3 (40)	210 ± 20 (40)	37 ± 4 (40)	19, 13–259
	−/−	−40.2 ± 0.9 (26)	5.7 ± 0.3 (26)	5.4 ± 0.3 (26)	1.11 ± 0.08 (26)	45, 14–277
Striola	+/+	−87 ± 3 (6)	4.3 ± 0.3 (6)	310 ± 70 (6)	41 ± 7 (6)	40, 15–59
	+/−	−88 ± 2 (3)	4.7 ± 0.9 (3)	270 ± 60 (3)	44 ± 6 (3)	19, 14–20
	−/−	−38 ± 1 (13)	6.2 ± 0.4 (13)	6.5 ± 0.6 (13)	1.5 ± 0.1 (13)	202, 14–370

*−/− vs +/+: two-way ANOVA, $p < 1E{-}9$, g 7.7; −/− vs +/−: two-way ANOVA, $p < 1E{-}9$, g 6.8.
[†]−/− vs +/+: two-way ANOVA, $p = 8.4E{-}4$, g 1.2.
[‡]−/− vs +/+: two-way ANOVA, $p < 1E{-}9$, g 3.7; −/− vs +/−: two-way ANOVA, $p < 1E{-}9$, g 2.1.
[§]−/− vs +/+: two-way ANOVA, $p < 1E{-}9$, g 3.6; −/− vs +/−: two-way ANOVA, $p < 1E{-}9$, g 2.0.

was identified as that remaining after 'blocking' $g_{K,L}$ with 20 mM external Ba^{2+}. Our new data suggest that there is no large non-$g_{K,L}$ conductance, and that instead high Ba^{2+} positively shifted the apparent voltage dependence of $g_{K,L}$.

$K_V1.8$ strongly affects type I passive properties and responses to current steps

While the cells of $Kcna10^{-/-}$ and $Kcna10^{+/-}$ epithelia appeared healthy, type I HCs had smaller membrane capacitances (C_m): 4–5 pF in $Kcna10^{-/-}$ type I HCs, ~20% smaller than $Kcna10^{+/-}$ type I HCs (~6 pF) and ~30% smaller than $Kcna10^{+/+}$ type I HCs (6–7 pF; *Table 2*). While C_m scales with surface area, the lack of change in soma sizes by deletion of $K_V1.8$ (*Supplementary file 1b*) suggests that surface area was not different. Instead, C may be higher in $Kcna10^{+/+}$ cells because of $g_{K,L}$ for two reasons. First, highly expressed trans-membrane proteins (see discussion of $g_{K,L}$ channel density in *Chen and Eatock, 2000*) can affect membrane thickness (*Mitra et al., 2004*), which is inversely proportional to specific C_m. Second, resistive current through $g_{K,L}$ could contaminate estimations of capacitive current, which is calculated from the decay time constant of transient current evoked by a small voltage step negative to –90 mV, where we measured C_m (see Methods).

Basolateral conductances help set the resting potential and passive membrane properties that regulate the time course and gain of voltage responses to small currents. To examine the effect of

Table 2. Type I hair cell passive membrane properties in the extrastriola (ES) and striola (S).
Mean ± SEM (number of cells). g is effect size, Hedge's g. KWA is Kruskal–Wallis ANOVA.

Zone	Kcna10	V_{rest}, mV*, [†]	R_{input}, MΩ[‡]	τ_{RC}, ms[§]	C_m, pF[¶]	Age (median, range)
ES	+/+	−84 ± 3 (6)	44 ± 6 (6)	0.24 ± 0.03 (6)	6.1 ± 0.4 (13)	20, 14–287
	+/−	−88.0 ± 0.7 (28)	55 ± 5 (24)	0.32 ± 0.03 (23)	5.8 ± 0.2 (44)	21, 16–29
	−/−	−63 ± 2 (15)	1400 ± 100 (15)	6.4 ± 0.6 (15)	5.0 ± 0.2 (27)	45, 14–202
S	+/+	−87 ± 2 (4)	50 ± 8 (4)	0.30 ± 0.04 (4)	7.4 ± 0.7 (7)	43, 40–59
	+/−	−87 ± 3 (3)	38 ± 8 (2)	0.21 ± 0.01 (2)	5.9 ± 0.6 (3)	19, 19–20
	−/−	−74 ± 5 (5)	1000 ± 300 (4)	4.2 ± 1.0 (4)	4.4 ± 0.2 (14)	202, 24–370

*Striolar −/− vs ES −/−: two-way ANOVA, $p = 0.006$, g 1.2; striolar −/− vs striolar +/+,+/−: two-way ANOVA, $p = 0.005$, g 1.7.
[†]−/− vs +/+: two-way ANOVA, $p < 1E{-}9$, g 2.3; −/− vs +/−: two-way ANOVA, $p < 1E{-}9$, g 3.4.
[‡]−/− vs +/+: two-way ANOVA, $p < 1E{-}9$, g 3.1; −/− vs +/−: two-way ANOVA, $p < 1E{-}9$, g 3.9.
[§†]−/− vs +/+: two-way ANOVA, $p < 1E{-}9$, g 2.7; −/− vs +/−: two-way ANOVA, $p < 1E{-}9$, g 3.4.
[¶‡]−/− vs +/+: two-way ANOVA, $p = 3E{-}7$, g 1.5; −/− vs +/−: two-way ANOVA, $p = 1.3E{-}4$, g 1.0; +/−vs +/+: two-way ANOVA, $p = 0.048$, g 0.6.
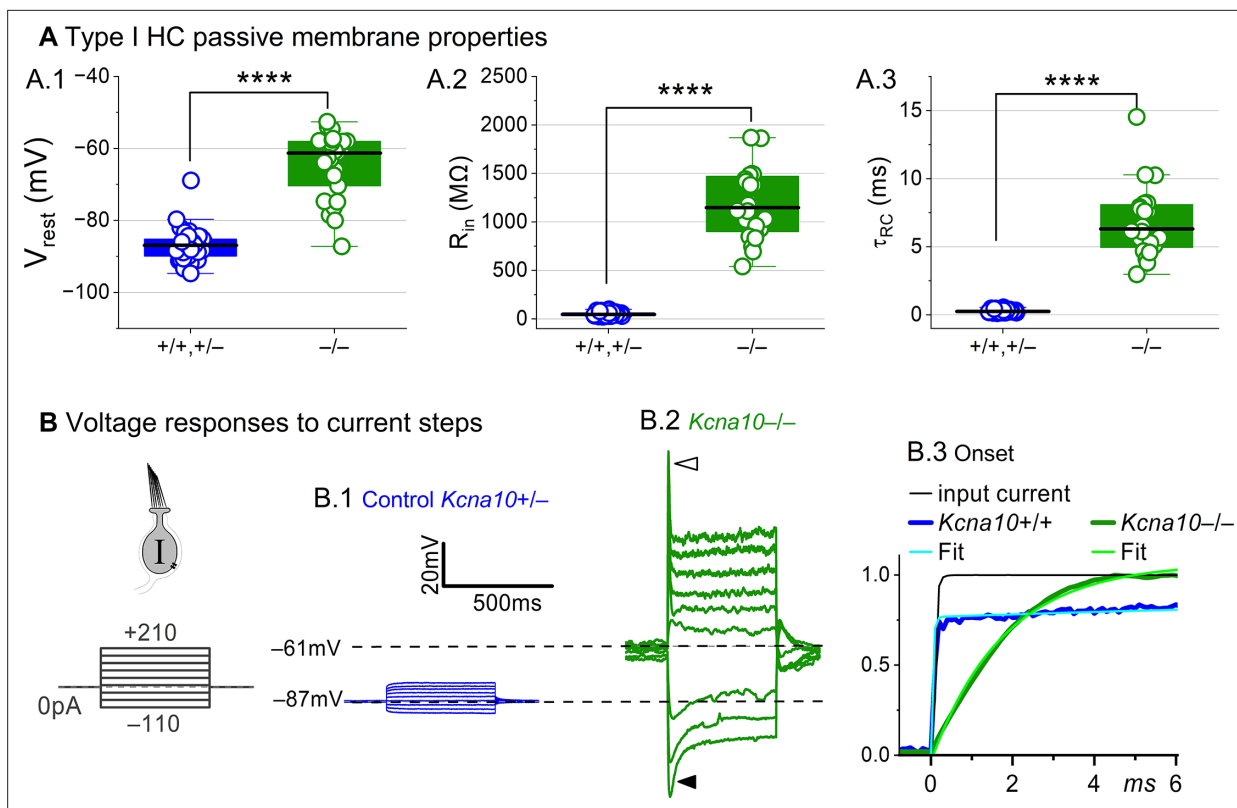
Figure 2. Kcna10$^{-/-}$ type I hair cells (HCs) had much longer membrane charging times and higher input resistances (voltage gains) than Kcna10$^{+/+,+/-}$ type I HCs. (**A**) g$_{K,L}$ strongly affects passive membrane properties: (**A.1**) V$_{rest}$, Tukey's test p<1E-9, (**A.2**) R$_{in}$, input resistance, Tukey's test p<1E-9, and (**A.3**) membrane time constant, $\tau_{RC} = (R_{input} * C_m)$, Tukey's test p<1E-9. See **Table 2** for all statistics. (**B**) Current clamp responses to the same scale from (**B.1**) Kcna10$^{+/-}$ and (**B.2**) Kcna10$^{-/-}$ type I cells, both P29. Filled arrowhead (B.2), sag indicating I$_H$ activation. Open arrowhead, Depolarization rapidly decays as I$_{DR}$ activates. (**B.3**) First 6 ms of voltage responses to 170 pA injection, normalized to steady-state value; curves, double-exponential fits (Kcna10$^{+/+}$, τ 40 μs and 2.4 ms) and single-exponential fits (Kcna10$^{-/-}$, τ 1.1 ms). Asterisks, ****p < 0.0001. Line, median; Box, interquartile range; Whiskers, outliers.

K$_V$1.8 on these properties, we switched to current clamp mode and measured resting potential (V$_{rest}$), input resistance (R$_{in}$, equivalent to voltage gain for small current steps, $\Delta V/\Delta I$), and membrane time constant (τ_{RC}). In Kcna10$^{-/-}$ type I HCs, V$_{rest}$ was much less negative (**Figure 2A.1**), R$_{in}$ was greater by ~20-fold (**Figure 2A.2**), and membrane charging times were commensurately longer (**Figure 2A.3**).

The differences between the voltage responses of Kcna10$^{+/+,+/-}$ and Kcna10$^{-/-}$ type I HCs are expected from the known impact of g$_{K,L}$ on V$_{rest}$ and R$_{in}$ (**Correia and Lang, 1990**; **Ricci et al., 1996**; **Rüsch and Eatock, 1996b**; **Songer and Eatock, 2013**). The large K$^+$-selective conductance at V$_{rest}$ holds V$_{rest}$ close to E$_K$ (K$^+$ equilibrium potential) and minimizes gain ($\Delta V/\Delta I$), such that voltage-gated conductances are negligibly affected by the input current and the cell produces approximately linear, static responses to iterated current steps. For Kcna10$^{-/-}$ type I HCs, with their less negative V$_{rest}$ and larger R$_{in}$, positive current steps evoked a fast initial depolarization (**Figure 2B.2**), activating residual delayed rectifiers and repolarizing the membrane toward E$_K$. Negative current steps evoked an initial hyperpolarization followed by a slowly repolarizing 'sag' (**Figure 2B.2**) as the HCN1 channels open (**Rüsch and Eatock, 1996b**; **Horwitz et al., 2011**).

Overall, comparison of the Kcna10$^{+/+,+/-}$ and Kcna10$^{-/-}$ responses shows that with K$_V$1.8 (g$_{K,L}$), the voltage response of the type I HC is smaller but better reproduces the time course of the input current.

K$_V$1.8 is necessary for both inactivating and non-inactivating K$_V$ currents in type II HCs

Type II HCs also express K$_V$1.8 mRNA (**McInturff et al., 2018**; **Orvis et al., 2021**). Although their outwardly rectifying conductances (g$_A$ and g$_{DR}$) differ substantially in voltage dependence and size

from $g_{K,L}$, both conductances were strongly affected by the null mutation: g_A was eliminated and the delayed rectifier was substantially smaller. Below we describe g_A and g_{DR} in $Kcna10^{+/+,+/-}$ type II HCs and the residual outward-rectifying current in $Kcna10^{-/-}$ type II HCs.

$Kcna10^{+/+,+/-}$ **type II HCs**. Most (81/84) $Kcna10^{+/+,+/-}$ type II HCs expressed a rapidly activating, rapidly inactivating A-type conductance (g_A). We define A current as the outwardly rectifying current that inactivates by over 30% within 200 ms. g_A was more prominent in extrastriolar zones, as reported (*Holt et al., 1999*; *Weng and Correia, 1999*).

We compared the activation and inactivation time course and inactivation prominence for 200 ms steps from –124 to ~30 mV. Outward currents fit with *Equation 3* yielded fast inactivation time constants ($\tau_{Inact,Fast}$) of ~30 ms in LES (*Figure 3A.2*). $\tau_{Inact,Fast}$ was faster in LES than in MES or striola (*Figure 3A.3*) and fast inactivation was a larger fraction of the total inactivation in LES than striola (~0.5 vs 0.3, *Figure 3A.4*).

To show voltage dependence of activation, we generated *G–V* curves for peak currents (sum of A-current and delayed rectifier) and steady-state currents measured at 200 ms, after g_A has mostly inactivated (*Figure 3D.2*). $Kcna10^{+/-}$ HCs had smaller currents than $Kcna10^{+/+}$ HCs, reflecting a smaller g_{DR} (*Figure 3D*) and faster fast inactivation (*Figure 3A.3*). As discussed later, these effects may relate to effects of the *Kcna10* gene dosage on the relative numbers of different $K_V1.8$ heteromers.

For $Kcna10^{+/+}$ and $Kcna10^{+/-}$ HCs, the voltage dependence as summarized by V_{half} and slope factor (S) was similar. Relative to g_{SS}, g_{Peak} had a more positive V_{half} (~–21 vs ~–26) and greater S (~12 vs ~9, *Figure 3D*, *Table 4*). Because g_{Peak} includes channels with and without fast inactivation, the shallower g_{Peak}–V curve may reflect a more heterogeneous channel population. Only g_{Peak} showed zonal variation, with more positive V_{half} in LES than striola (~–20 vs ~–24 mV, *Figure 3D*, *Table 4*). We later suggest that variable subunit composition may drive zonal variation in g_{Peak}.

$Kcna10^{-/-}$ **type II HCs**. $Kcna10^{-/-}$ type II HCs from all zones were missing g_A and 30–50% of g_{DR} (*Figure 3B–D*). The residual delayed rectifier (1.3 nS/pF) had a more positive V_{half} than g_{DR} in $Kcna10^{+/+,+/-}$ HCs (~–20 vs ~–26 mV, *Figure 3D.2*). We refer to the $K_V1.8$-dependent delayed rectifier component as $g_{DR}(K_V1.8)$ and to the residual, $K_V1.8$-independent delayed rectifier component as $g_{DR}(K_V7)$ because, as we show later, it includes K_V7 channels.

Figure 3—figure supplement 2 shows the development of $K_V1.8$-dependent and -independent K_V currents in type II HCs with age from P5 to over P300. In $Kcna10^{+/+,+/-}$ type II HCs, g_A was present at all ages with a higher % inactivation after P18 than at P5–P10 (*Figure 3—figure supplement 2A.4*). g_{Peak} did not change much above P12 except for a compression of conductance density from P13 to P370 (partial correlation coefficient = –0.4, p = 2E−5, *Figure 3—figure supplement 2A.3*).

We saw small rapidly inactivating outward currents in a minority of $Kcna10^{-/-}$ type II HCs (23%, 7/30), all >P12 and extrastriolar (*Figure 3—figure supplement 3*). These currents overlapped with g_A in percent inactivation, inactivation kinetics, and activation voltage dependence but were very small. As discussed later, we suspect that these currents flow through homomers of inactivating K_V subunits that in control HCs join with $K_V1.8$ subunits and confer inactivation on the heteromeric conductance.

$K_V1.8$ affects type II passive properties and responses to current steps

In type II HCs, absence of $K_V1.8$ did not change V_{rest} (*Figure 4A.1*) because g_A and g_{DR} both activate positive to rest, but significantly increased R_{in} and τ_{RC} (*Figure 4A.2 and A.3*).

Positive current steps evoked an initial depolarizing transient in both $Kcna10^{+/+}$ and $Kcna10^{-/-}$ type II HCs, but the detailed time course differed (*Figure 4B*). Both transient and steady-state responses were larger in $Kcna10^{-/-}$, consistent with their larger R_{in} values.

Absence of $K_V1.8$ increased the incidence of sharp electrical resonance in type II HCs. Electrical resonance, which manifests as ringing responses to current steps, can support receptor potential tuning (*Ashmore, 1983*; *Fettiplace, 1987*; *Hudspeth and Lewis, 1988*; *Ramanathan and Fuchs, 2002*). Larger R_{in} values made $Kcna10^{-/-}$ type II HCs more prone to electrical resonance; *Figure 4C.1* shows a striking example. Median resonance quality (Q_e, sharpness of tuning) was greater in $Kcna10^{-/-}$ (1.33, n=26) than $Kcna10^{+/+}$ (0.66, n = 23) or $Kcna10^{+/-}$ (0.59, n = 44) type II HCs.

$K_V1.8$ affected the time course of the initial peak in response to much larger current injections (*Figure 4D, E*). Fast activation of g_A in control type II HCs rapidly repolarizes the membrane and then inactivates, allowing the constant input current to progressively depolarize the cell, producing a slow
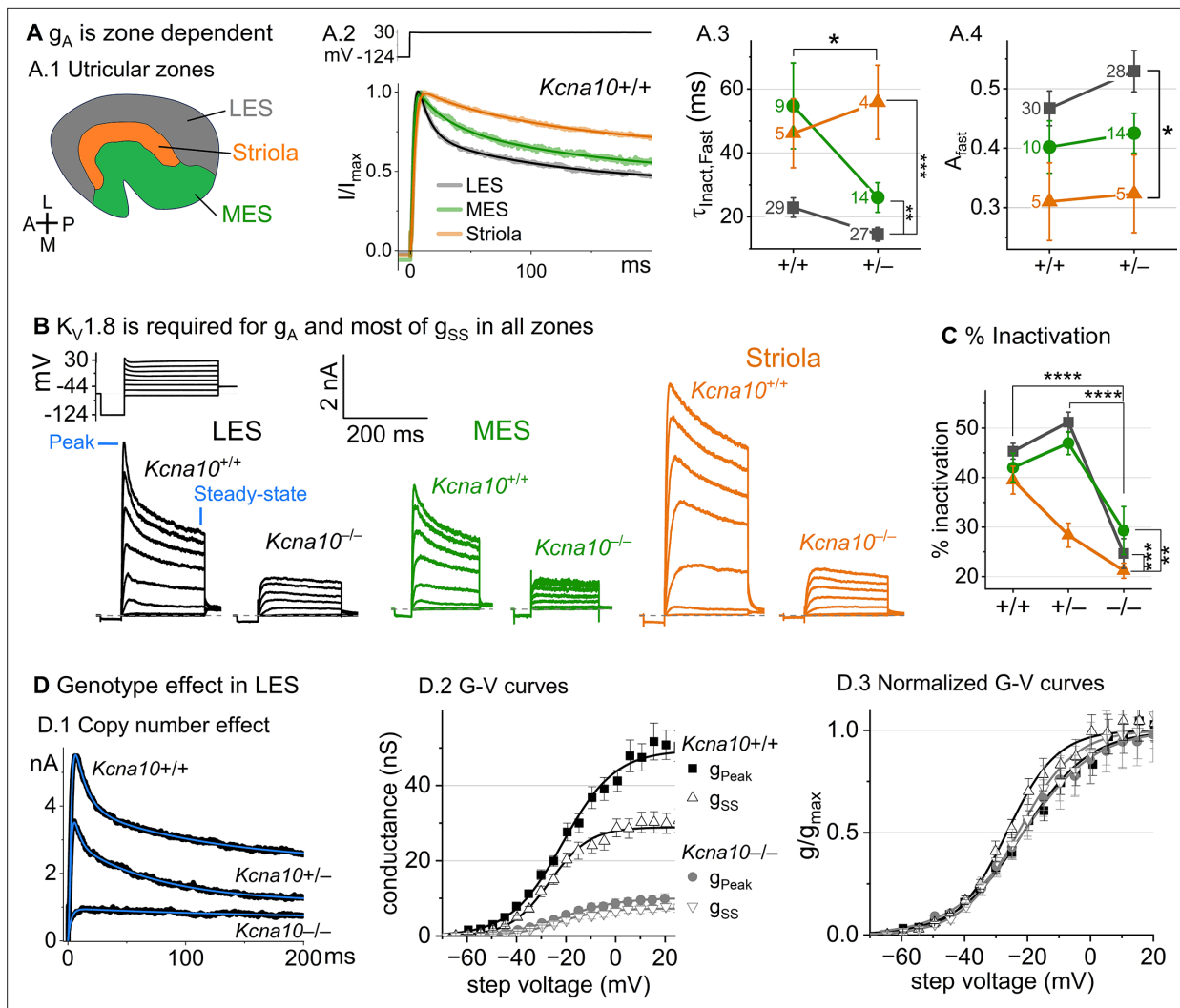
Figure 3. $Kcna10^{-/-}$ type II hair cells (HCs) in all zones of the sensory epithelium lacked the major rapidly inactivating conductance, g_A, and had less delayed rectifier conductance. Activation and inactivation varied with epithelial zone and genotype. (**A**) g_A inactivation time course varied across zones. (**A.1**) Zones of the utricular epithelium: lateral extrastriola (LES), medial extrastriola (MES), and striola (S). (**A.2**) Normalized currents evoked by steps from –124 to +30 mV with overlaid fits of *Equation 3*. (**A.3**) $\tau_{Inact,Fast}$ was faster in $Kcna10^{+/-}$ (n=45) than $Kcna10^{+/+}$ (n=43) HCs (KWA, p=0.027), and faster in LES (n=56) than MES (n=23, KWA, p=0.002) or S (n=9, KWA, p=2E-4). Point label is number of cells. Brackets show post hoc pairwise comparisons between two zones (vertical brackets) and horizontal brackets compare two genotypes; see *Table 3* for statistics on kinetics. (**A.4**) Fast inactivation was a greater fraction of total inactivation in LES (n=58) than striola (n=10, Tukey's test p=0.0041). (**B**) Exemplars; ages, *left to right*, P312, P53, P287, P49, P40, P154. (**C**) % inactivation at 30 mV was much lower in $Kcna10^{-/-}$ (n=37) than $Kcna10^{+/-}$ (n=47, Tukey's HSD, p<1E-9) and $Kcna10^{+/+}$ (n=44, Tukey's HSD, p<1E-9). % inactivation was lower in striola (n=16) than LES (n=77, Tukey's HSD, p=3E-5) and MES (n=36, Tukey's HSD, p=0.0011). 2-way ANOVA detected interaction between zone and genotype, p=0.026 (*Table 3*). (**D**) Exemplar currents and *G–V* curves from LES type II HCs show a copy number effect. (**D.1**) Exemplar currents evoked by steps from –124 to +30 mV fit with *Equation 3*. (**D.2**) Averaged peak and steady-state conductance–voltage data points from LES cells (+/+, n=37; –/–, n=20) were fit with Boltzmann equations (*Equation 1*) and normalized by g_{max} in (**D.3**). *Asterisks*: *p < 0.05; **p < 0.01; ***p < 0.001; and ****p < 0.0001. *Error bars*, SEM. See *Table 4* for statistics on voltage dependence.

The online version of this article includes the following figure supplement(s) for figure 3:

Figure supplement 1. For type II hair cells (HCs) older than P12, K_V conductance activation and inactivation differed across zones and genotypes.

Figure supplement 2. For type II hair cells (HCs) older than P12, K_V conductances were stable.

Figure supplement 3. A minority of extrastriolar $Kcna10^{-/-}$ type II hair cells (HCs) had a very small fast-inactivating outward rectifier current.

Table 3. Type II hair cell K_V currents: activation and inactivation time course at +30 mV. Mean ± SEM. g is effect size, Hedge's g. KWA is Kruskal–Wallis ANOVA.

Zone	Kcna10	τ_{Act} at 30 mV, ms[*, †]	$\tau_{Inact,Fast}$ at 30 mV, ms [‡, §]	Fast inactivation prominence[¶]	Inactivation %[**,††]	N cells	Age (median, range)
LES	+/+	2.11 ± 0.09	23 ± 3	0.46 ± 0.03	45 ± 2	30	46, 14–312
	+/–	1.64 ± 0.09	15 ± 2	0.53 ± 0.03	51 ± 2	27	29, 13–280
	–/–	4.4 ± 0.5	NA	NA	25 ± 3	21	128, 15–355
MES	+/+	2.8 ± 0.5	50 ± 10	0.40 ± 0.04	42 ± 3	9	94, 22–296
	+/–	2.2 ± 0.2	90 ± 60	0.42 ± 0.03	47 ± 2	15	24, 13–52
	–/–	10 ± 7	NA	NA	29 ± 5	10	84, 28–355
Striola	+/+	2.7 ± 0.3	50 ± 10	0.31 ± 0.07	39 ± 3	5	45, 40–287
	+/–	2.9 ± 0.4	300 ± 200	0.3 ± 0.06	28 ± 2	5	19, 14–30
	–/–	7 ± 2	NA	NA	22 ± 2	6	202, 29–298

[*]–/– vs +/+: KWA, p = 0.0048, g 0.6; –/– vs +/–: KWA, p = 2.3E−7, g 0.6.

[†]Striola vs LES: KWA, p = 5.7E−4, g 1.0.

[‡]+/– vs +/+: KWA, p = 0.027, g 0.2.

[§]LES vs MES: KWA, p = 0.0018, g 0.3; LES vs Striola: KWA, p = 1.9E−4, g 0.8.

[¶]LES vs Striola: two-way ANOVA, p = 0.0041, g 0.7.

[**]–/– vs +/+: two-way ANOVA, p < 1E−9, g 1.7; –/– vs +/–: two-way ANOVA, p < 1E−9, g 1.8.

[††]Striola vs LES: two-way ANOVA, p = 3.4E−5, g 0.9; Striola vs MES: two-way ANOVA, p = 0.0011, g 1.0; interaction between genotype and zone: two-way ANOVA, p = 0.026.

rebound (*Figure 4D.2*). This behavior has the potential to counter mechanotranduction adaptation (*Vollrath and Eatock, 2003*).

K_V1.8 immunolocalized to basolateral membranes of both type I and II HCs

If K_V1.8 is a pore-forming subunit in the K_V1.8-dependent conductances $g_{K,L}$, g_A, and g_{DR}, it should localize to HC membranes. *Figure 5* compares K_V1.8 immunoreactivity in $Kcna10^{+/+}$ and $Kcna10^{-/-}$ utricles, showing specific immunoreactivity along the basolateral membranes of both HC types in $Kcna10^{+/+}$ utricles. To identify HC type and localize the HC membrane, we used antibodies against K_V7.4 (KCNQ4), an ion channel densely expressed in the calyceal 'inner-face' membrane next to the synaptic cleft (*Hurley et al., 2006*; *Lysakowski et al., 2011*), producing a cup-like stain around type I HCs (*Figure 5A*). K_V1.8 immunoreactivity was present in HC membrane apposing K_V7.4-stained calyx inner face in $Kcna10^{+/+}$ utricles (*Figure 5A.1 and A.2*) and not in $Kcna10^{-/-}$ utricles (*Figure 5A.3*).

In other experiments, we used antibodies against calretinin (CALB2), a cytosolic calcium-binding protein expressed by many type II HCs and also by striolar calyx-only afferents (*Desai et al., 2005*; *Lysakowski et al., 2011*, *Figure 5B*). An HC is type II if it is calretinin-positive (*Figure 5B.1*) or if it lacks a K_V7.4- or calretinin-positive calyceal cup (*Figure 5A.2 and B.3*, rightmost cells). HC identification was confirmed with established morphological indicators: for example, type II HCs tend to have basolateral processes (feet) (*Pujol et al., 2014*) and, in the extrastriola, more apical nuclei than type I HCs.

Previously, *Carlisle et al., 2012* reported K_V1.8-like immunoreactivity in many cell types in the inner ear. In contrast, *Lee et al., 2013* found that gene expression reporters indicated expression only in HCs and some supporting cells. Here, comparison of control and null tissue showed selective expression of HC membranes, and that some supporting cell staining is non-specific.

K_V1.4 may also contribute to g_A

Results with the K_V1.8 knockout suggest that type II HCs have an inactivating K_V1 conductance that includes K_V1.8 subunits. K_V1.8, like most K_V1 subunits, does not show fast inactivation as a heterologously expressed homomer (*Lang et al., 2000*; *Ranjan et al., 2019*; *Dierich et al., 2020*), nor do the K_V1.8-dependent channels in type I HCs, as we show, and in cochlear inner HCs (*Dierich et al., 2020*).

Table 4. Type II hair cell K_V currents: activation voltage dependence.
Mean ± SEM. g is effect size, Hedge's g. KWA is Kruskal–Wallis ANOVA.

Zone	Kcna10	Peak $V_{1/2}$, mV**	Peak S, mV†† ‡	A-type g_{max}/C_m, nS/pF§ §	SS V_{half}, mV¶ ¶	SS S, mV****	SS g_{max}/C_m, nS/pF †† ‡‡	N cells	Age (median, range)
LES	+/+	−19.8 ± 0.6	11.8 ± 0.4	4.0 ± 0.3	−25.0 ± 0.5	8.7 ± 0.3	7.1 ± 0.8	37	46, 14–312
	+/−	−19.8 ± 0.8	12.8 ± 0.4	3.8 ± 0.3	−26.8 ± 0.8	8.7 ± 0.3	4.9 ±0.4	35	29, 13–280
	−/−	−18 ± 1	11.7 ± 0.4	0.37 ± 0.05	−19 ± 1	12.1 ± 0.5	1.8 ±0.2	20	128, 15–355
MES	+/+	−22 ± 1	11 ± 0.7	4.1 ± 0.7	−26 ± 1	8.3 ± 0.5	9 ±1	11	94, 22–296
	+/−	−21 ± 1	11.8 ± 0.4	3.6 ± 0.5	−27 ± 1	9.0 ± 0.3	5.9 ±0.7	16	24, 13–52
	−/−	−19 ± 1	10.8 ± 0.6	0.6 ± 0.1	−20 ± 1	10.7 ± 0.7	2.5 ±0.3	15	84, 28–355
Striola	+/+	−24 ± 1	9.6 ± 0.5	5 ± 1	−26.6 ± 0.9	8.2 ± 0.4	12 ±1	7	45, 40–287
	+/−	−25 ± 2	9.4 ± 0.4	2.6 ± 0.6	−28 ± 2	8.2 ± 0.3	10±2	6	19, 14–30
	−/−	−21.3 ± 0.9	10.3 ± 0.5	0.7 ± 0.1	−21.7 ± 0.8	10.5 ± 0.6	3.9±0.5	8	202, 29–298

*Striola vs LES: two-way ANOVA, p = 0.00116, g 0.9.
†Striola vs MES: two-way ANOVA, p = 0.016, g 0.8; Striola vs LES: two-way ANOVA, p = 7.5E−6, g 1.2.
‡−/− vs +/−: two-way ANOVA, p = 0.036, g 0.5.
§−/− vs +/+: Welch ANOVA, p < 1E−9, g 2.3; −/− vs +/−: Welch ANOVA, p < 1E−9, g 2.3.
¶−/− vs +/+: two-way ANOVA, p < 1E−9, g 1.4; −/− vs +/−: two-way ANOVA, p < 1E−9, g 1.6.
**−/− vs +/+: two-way ANOVA, p < 1E−9, g 1.4; −/− vs +/−: two-way ANOVA, p = 4.5E−7, g 1.1.
††−/− vs +/+: Welch ANOVA, p < 1E−9, g 1.6; −/− vs +/−: Welch ANOVA, p < 1E−9, g 1.3; +/+vs +/−: Welch ANOVA, p = 0.007, g 1.6.
‡‡Striola vs LES: one-way ANOVA, p = 0.001, g (0.9); Striola vs MES: one-way ANOVA, p = 0.01, g 0.8.

$K_V 1$ subunits without intrinsic inactivation can produce rapidly inactivating currents by associating with $K_V \beta 1$ or $K_V \beta 3$ subunits. $K_V \beta 1$ (*Kcnb1*) is present in type II HCs alongside $K_V \beta 2$ (*Kcnb2*) (*McInturff et al., 2018*; *Jan et al., 2021*; *Orvis et al., 2021*), which does not confer rapid inactivation (*Dwenger et al., 2022*).

Another possibility is that in type II HCs, $K_V 1.8$ subunits heteromultimerize with $K_V 1.4$ subunits—the only $K_V 1$ subunits which, when expressed as a homomer, have complete N-type (fast) inactivation (*Stühmer et al., 1989*). Multiple observations support this possibility. $K_V 1.4$ has been linked to g_A in pigeon type II HCs (*Correia et al., 2008*) and is the second-most abundant $K_V 1$ transcript in mammalian

Table 5. Type II hair cell passive membrane properties in the extrastriola (ES) and striola (S). Mean ± SEM (number of cells). g is effect size, Hedge's g. KWA is Kruskal–Wallis ANOVA. Peak height and time were measured from responses to 170 pA input from rest.

Zone	Kcna10	V_{rest}, mV	R_{input}, GΩ*	τ_{RC}, ms†	Peak height, mV‡	Peak time, ms§	C_m, pF	Age (median, range)
ES	+/+	−71 ± 2 (19)	1.4 ± 0.2 (16)	11 ± 3 (16)	−20 ± 2 (15)	2.5 ± 0.2 (15)	4.7 ± 0.2 (50)	45, 16–312
	+/−	−71 ± 2 (34)	1.2 ± 0.1 (27)	9 ± 1 (27)	−20 ± 1 (30)	2.44 ± 0.08 (30)	4.6 ± 0.1 (52)	27, 13–280
	−/−	−76 ± 2 (9)	2.3 ± 0.3 (7)	16 ± 3 (7)	2 ± 6 (7)	3.6 ± 0.3 (7)	4.6 ± 0.2 (35)	53, 15–154
S	+/+	−73.1 ± 1.0 (6)	1.4 ± 0.1 (6)	9 ± 1 (6)	−20 ± 2 (5)	2.7 ± 0.1 (5)	4.6 ± 0.2 (7)	45, 40–224
	+/−	−71 ± 3 (5)	1.4 ± 0.3 (6)	7 ± 2 (6)	−20 ± 2 (6)	2.3 ± 0.1 (6)	4.8 ± 0.2 (6)	19, 19–30
	−/−	−68 ± 2 (6)	3.0 ± 0.7 (6)	26 ± 10 (6)	2 ± 7 (4)	4 ± 1 (4)	4.4 ± 0.3 (7)	178, 29–298

*−/− vs +/+: KWA, p = 0.015, g 1.2; −/− vs +/−: KWA, p = 0.002, g 1.5.
†−/− vs +/+: KWA, p = 0.016, g 0.7; −/− vs +/−: KWA, p = 0.008, g 1.2.
‡−/− vs +/+: KWA, p = 0.006, g 2.1; −/− vs +/−: KWA, p = 2E−4, g 2.6.
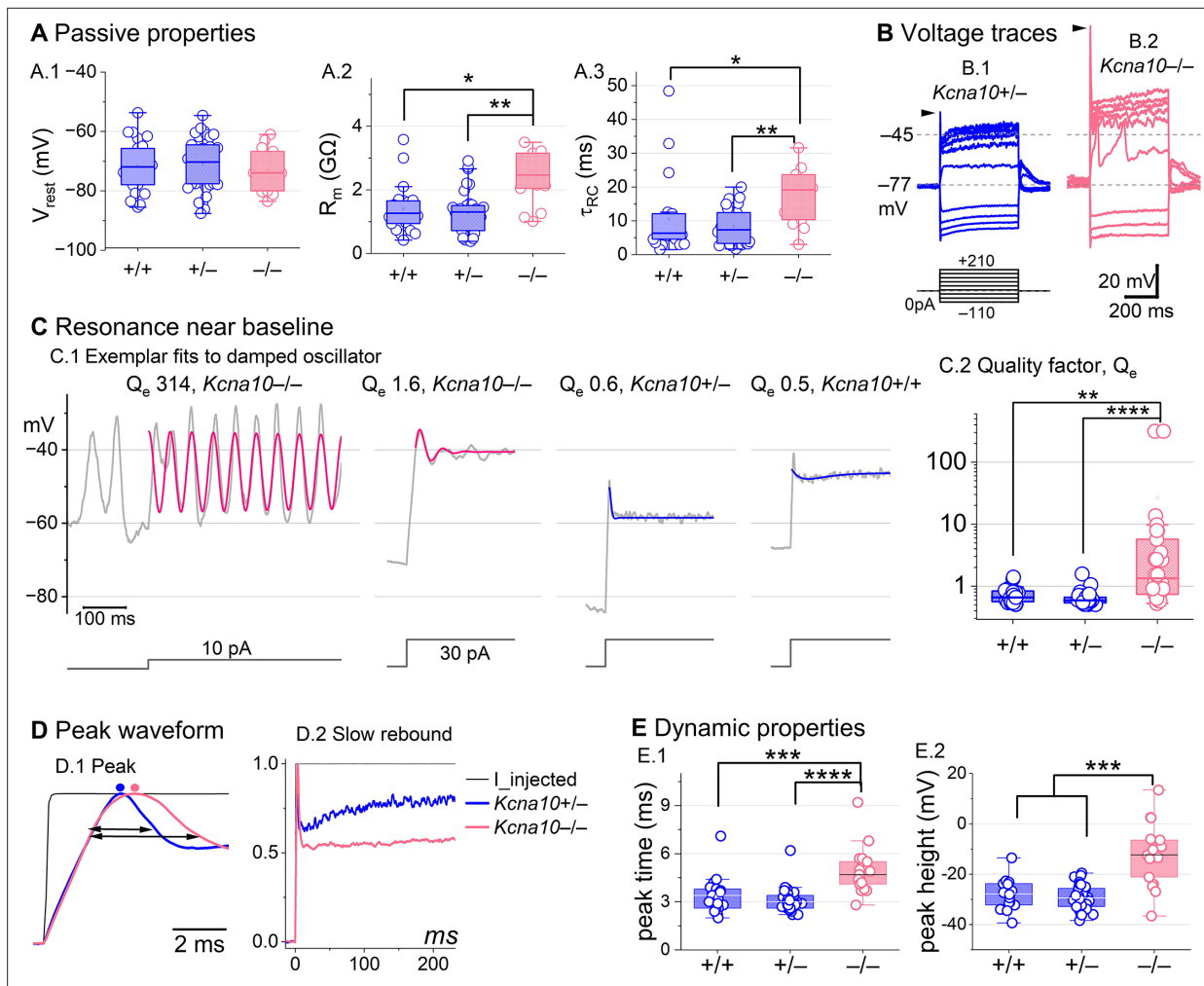§−/− vs +/+: two-way ANOVA, p < 1E−9, g 1.3; −/− vs +/−: two-way ANOVA, p < 1E−9, g 1.9.

Figure 4. *Kcna10^{−/−}* type II hair cells (HCs) had larger, slower voltage responses and more electrical resonance. (**A**) Passive membrane properties near resting membrane potential: (**A.1**) Resting potential. R_{input} (**A.2**) and τ_{RC} (**A.3**) were obtained from single-exponential fits to voltage responses <15 mV. R_{input} and τ_{RC} were higher in *Kcna10^{−/−}* (n=13) than *Kcna10^{+/+}* (n=22, KWA p=0.015; p=0.016) and *Kcna10^{+/−}* (n=33, KWA p=0.002; p=0.008; see *Table 5*). (**B**) Exemplar voltage responses to iterated current steps (*bottom*) illustrate key changes in gain and resonance with $K_V1.8$ knockout. (**B.1**) *Kcna10^{+/−}* type II HC (P24, LES) and (**B.2**) *Kcna10^{−/−}* type II HC (P53, LES). Arrowheads, depolarizing transients. (**C**) Range of resonance illustrated for *Kcna10^{−/−}* type II HCs (*left, pink curves fit to* **Equation 5**) and controls (*right, blue fits*). (**C.1**) *Resonant frequencies, left to right:* 19.6, 18.4, 34.4, and 0.3 Hz. Leftmost cell resonated spontaneously (before step). (**C.2**) Tuning quality (Q_e; **Equation 6**) was higher for *Kcna10^{−/−}* (n=26) type II HCs (KWA: p = 0.0064 vs *Kcna10^{+/+}*, n=23; p = 7E-8 vs *Kcna10^{+/−}*, n=45). (**D**) *Kcna10^{−/−}* type II HCs had higher, slower peaks and much slower rebound potentials in response to large (170 pA) current steps. (**D.1**) Normalized to show initial depolarizing transient (*filled circles*, times of peaks; *horizontal arrows*, peak width at half-maximum). (**D.2**) Longer time scale to highlight how null mutation reduced post-transient rebound. (**E**) In *Kcna10^{−/−}* HCs (n=19), depolarizing transients evoked by a +90 pA step were slower to peak (**E.1**) than in *Kcna10^{+/+}* (n=19, 2-way ANOVA Tukey's p<1E-9) and *Kcna10^{+/−}* (n=34, 2-way ANOVA Tukey's p<1E-9) and (**E.2**) larger than in *Kcna10^{+/+}* (n=19, KWA p=0.006) and *Kcna10^{+/−}* (n=34, KWA p=2E-4). *Asterisks*: *p < 0.05; **p < 0.01; ***p < 0.001; and ****p < 0.0001. *Line*, median; *Box*, interquartile range; *Whiskers*, outliers.

vestibular HCs, after $K_V1.8$ (*Scheffer et al., 2015*). $K_V1.4$ is expressed in type II HCs but not type I HCs (*McInturff et al., 2018*; *Orvis et al., 2021*), and is not found in striolar HCs (*Jan et al., 2021*; *Orvis et al., 2021*), where even in type II HCs, inactivation is slower and less extensive (*Figure 3A*).

Functional heteromers form between $K_V1.4$ and other $K_V1.x$ and/or $K_V\beta1$ (*Imbrici et al., 2006*; *Correia et al., 2008*; *Al Sabi et al., 2011*). Although $K_V1.4$ and $K_V1.8$ heteromers have not been studied directly, g_A's inactivation time course ($\tau_{Fast,Inact}$ of ~30 ms +30 mV, *Figure 3A*) and voltage dependence (V_{half} –41 mV, *Figure 6B*) are consistent with these other $K_V1.4$-containing heteromers.
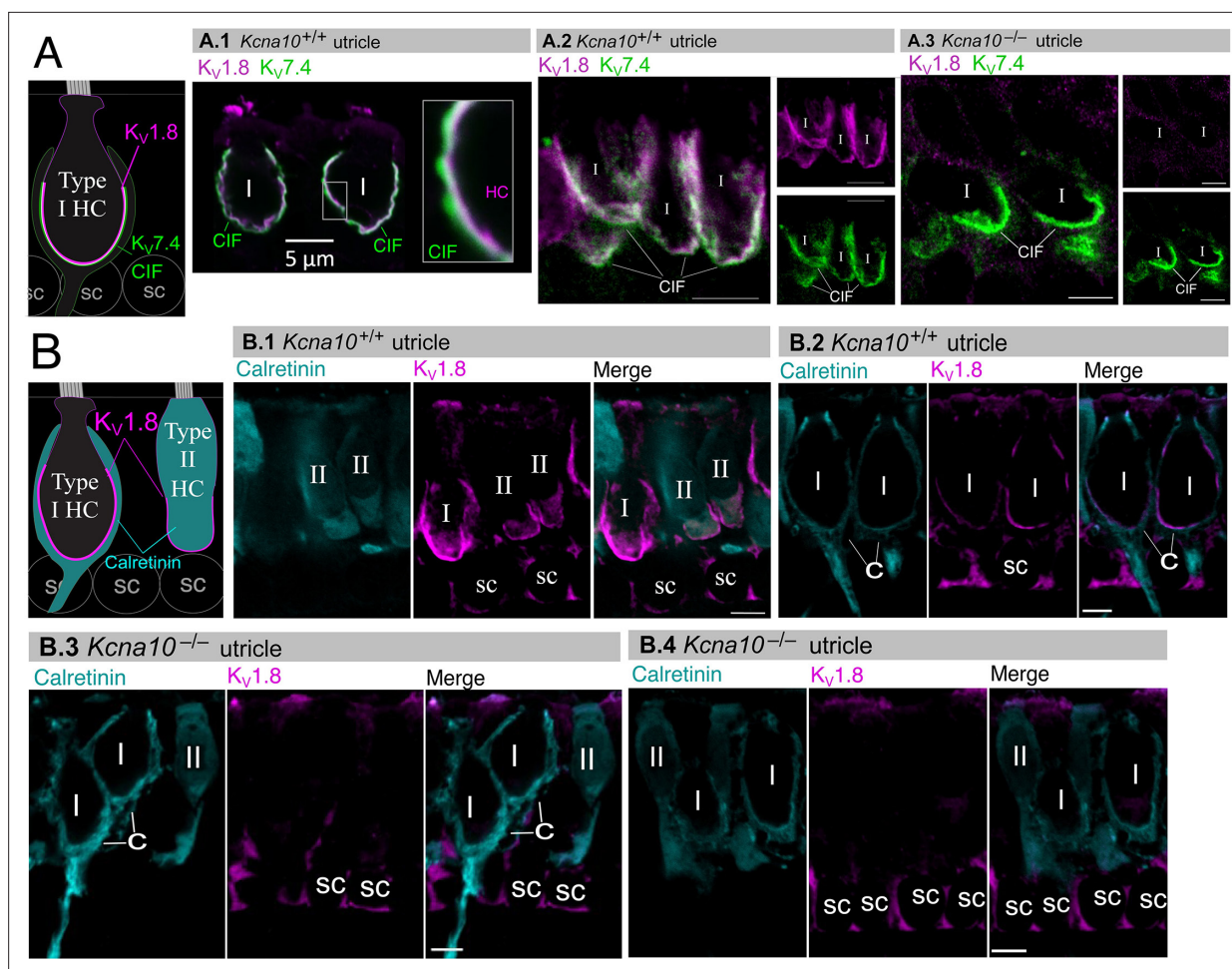
Figure 5. Type I and II hair cell (HC) basolateral membranes show specific immunoreactivity to Kv1.8 antibody (magenta). Antibodies for $K_V7.4$ (A, green) and calretinin (B, cyan) were used as counterstains for calyx membrane (Kv7.4), type II HC cytoplasm (calretinin) and cytoplasm of striolar calyx-only afferents (calretinin). (**A**) *Left*, Cartoon showing $K_V7.4$ on the calyx inner face membrane (CIF) and $K_V1.8$ on the type I HC membrane. SC, supporting cell nuclei. *A.1–3*, Adult mouse utricle sections. $K_V7.4$ antibody labeled calyces on two $K_V1.8$-positive type I HCs (*A.1*), four $K_V1.8$-positive type I HCs (*A.2*), and two $K_V1.8$-negative type I HCs from a *Kcna10⁻/⁻* mouse (*A.3*). (**B**) *Left*, Cartoon showing cytoplasmic calretinin stain in calyx-only striolar afferents and most type II HCs, and $K_V1.8$ on membranes of both HC types. In wildtype utricles, $K_V1.8$ immunolocalized to basolateral membranes of type I and II HCs (extrastriola, *B.1*). $K_V1.8$ immunolocalized to type I HCs (striola, *B.2*). Staining of supporting cell (SC) membranes by Kv1.8 antibody was non-specific, as it was present in *Kcna10⁻/⁻* tissue (striola, *B.3* and *B.4*). All scale bars 5 μm.

K_V7 channels contribute a small delayed rectifier in type I and II HCs

In *Kcna10⁻/⁻* HCs, absence of $I_{K,L}$ and I_A revealed smaller delayed rectifier K⁺ currents that, unlike $I_{K,L}$, activated positive to resting potential and, unlike I_A, lacked fast inactivation. Candidate channels include members of the K_V7 (KCNQ, M-current) family, which have been identified previously in rodent vestibular HCs (*Kharkovets et al., 2000*; *Rennie et al., 2001*; *Hurley et al., 2006*; *Scheffer et al., 2015*).

We tested for K_V7 contributions in *Kcna10⁻/⁻* type I HCs, *Kcna10⁻/⁻* type II HCs, and *Kcna10⁺/⁺,⁺/⁻* type II HCs of multiple ages by applying XE991 at 10 μM (*Figure 7A*), a dose selective for K_V7 channels (*Brown et al., 2002*) and close to the IC_{50} (*Alexander et al., 2019*). In *Kcna10⁻/⁻* HCs of both types, 10 μM XE991 blocked about half of the residual K_V conductance (*Figure 7B.1*), consistent with K_V7 channels conducting most or all of the non-$K_V1.8$ delayed rectifier current. In all tested HCs (P8–355, median P224), the XE991-sensitive conductance did not inactivate substantially within 200 ms at any voltage, consistent with $K_V7.2$, 7.3, 7.4, and 7.5 currents (*Wang, 1998*; *Kubisch et al., 1999*; *Schroeder et al., 2000*; *Jensen et al., 2007*; *Xu et al., 2007*). We refer to this component as $g_{DR}(K_V7)$. The voltage dependence and g_{max} density (g_{max}/C_m) of $g_{DR}(K_V7)$ were comparable across HC types
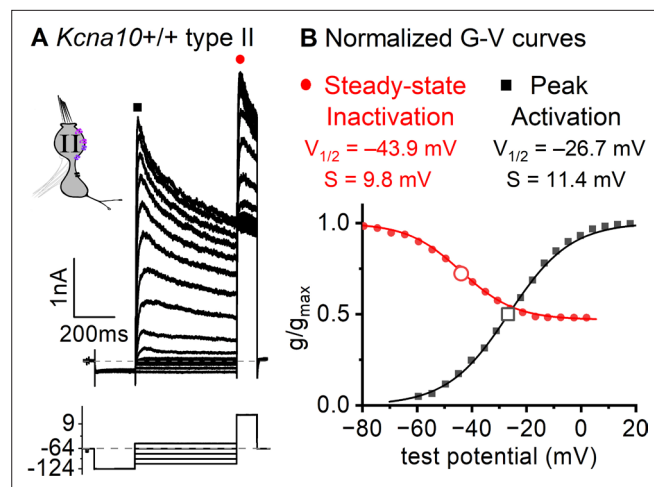
Figure 6. Inactivation curve of g_A in extrastriolar type II hair cells (HCs). (**A**) Modified voltage protocol measured accumulated steady-state inactivation at the tail potential. 100 µM ZD7288 in bath prevented contamination by HCN current. (**B**) Voltage dependence of g_A's steady-state inactivation (h_∞ curve) and peak activation are consistent with $K_V 1.4$ heteromers. *Curves*, Boltzmann fits (***Equation 1***). *Average fit parameters from Kcna10$^{+/+,+/-}$ type II HCs*, P40–P210, median P94. Inactivation: V_{half}, -42 ± 2 mV ($n = 11$); S, 11 ± 1 mV. Activation: V_{half}, -23 ± 1 mV ($n = 11$); S, 11.2 ± 0.4 mV.

and genotypes (***Figure 7B.2–4***). Although $K_V 7.4$ was not detectable in HCs during immunostaining (***Figure 5***), $K_V 7.4$ has been shown in type I HCs with immunogold labeling (***Kharkovets et al., 2000***; ***Hurley et al., 2006***).

These results are consistent with similar $K_V 7$ channels contributing a relatively small delayed rectifier in both HC types. In addition, the similarity of XE991-sensitive currents of *Kcna10$^{+/+}$* and *Kcna10$^{-/-}$* type II HCs indicates that knocking out $K_V 1.8$ did not cause general effects on ion channel expression. We did not test XE991 on *Kcna10$^{+/+,+/-}$* type I HCs because $g_{K,L}$ runs down in ruptured patch recordings (***Rüsch and Eatock, 1996a***; ***Chen and Eatock, 2000***; ***Hurley et al., 2006***), which could contaminate the XE991-sensitive conductance obtained by subtraction.

In one striolar *Kcna10$^{-/-}$* type I HC, XE991 also blocked a small conductance that activated negative to rest (***Figure 7—figure supplement 1A, B***). This conductance ($V_{half} \sim = -100$ mV, ***Figure 7—figure supplement 1C***) was detected only in *Kcna10$^{-/-}$* type I HCs from the striola (5/23 vs 0/45 extrastriolar). The V_{half} and $\tau_{deactivation}$ were similar to values reported for $K_V 7.4$ channels in cochlear HCs (***Wong et al., 2004***; ***Dierich et al., 2020***). This very negatively activating $K_V 7$ conductance coexisted with the larger more positively activating $K_V 7$ conductance (***Figure 7—figure supplement 1C***) and was too small (<0.5 nS/pF) to contribute significantly to $g_{K,L}$ (~10–100 nS/pF, ***Figure 1D***).

Other channels

While our data are consistent with $K_V 1.8$- and $K_V 7$-containing channels carrying most of the outward-rectifying current in mouse utricular HCs, there is evidence in other preparations for additional channels, including $K_V 11$ (KCNH, Erg) channels in rat utricular type I HCs (***Hurley et al., 2006***) and BK (KCNMA1) channels in rat utricle and rat and turtle semicircular canal HCs (***Schweizer et al., 2009***; ***Contini et al., 2020***).

BK is expressed in mouse utricular HCs (***McInturff et al., 2018***; ***Jan et al., 2021***; ***Orvis et al., 2021***). However, Ca^{2+}-dependent currents have not been observed in mouse utricular HCs, and we found little to no effect of the BK-channel blocker iberiotoxin at a dose (100 nM) well beyond the IC$_{50}$: percent blocked at –30 mV was $2 \pm 6\%$ (3 *Kcna10$^{-/-}$* type I HCs); $1 \pm 5\%$ (5 *Kcna10$^{+/+,+/-}$* type II HCs); 7% and 14% (2 *Kcna10$^{-/-}$* type II HCs). We also did not see N-shaped *I–V* curves typical of many Ca^{2+}-dependent K$^+$ currents. In our ruptured-patch recordings, Ca^{2+}-dependent BK currents and erg channels may have been eliminated by wash-out of the HCs' small Ca$_V$ currents (***Bao et al., 2003***) or cytoplasmic second messengers (***Hurley et al., 2006***).

To check whether the constitutive $K_V 1.8$ knockout has strong non-specific effects on channel trafficking, we examined the summed HCN and fast inward rectifier currents (I_H and I_{Kir}) at –124 mV, and
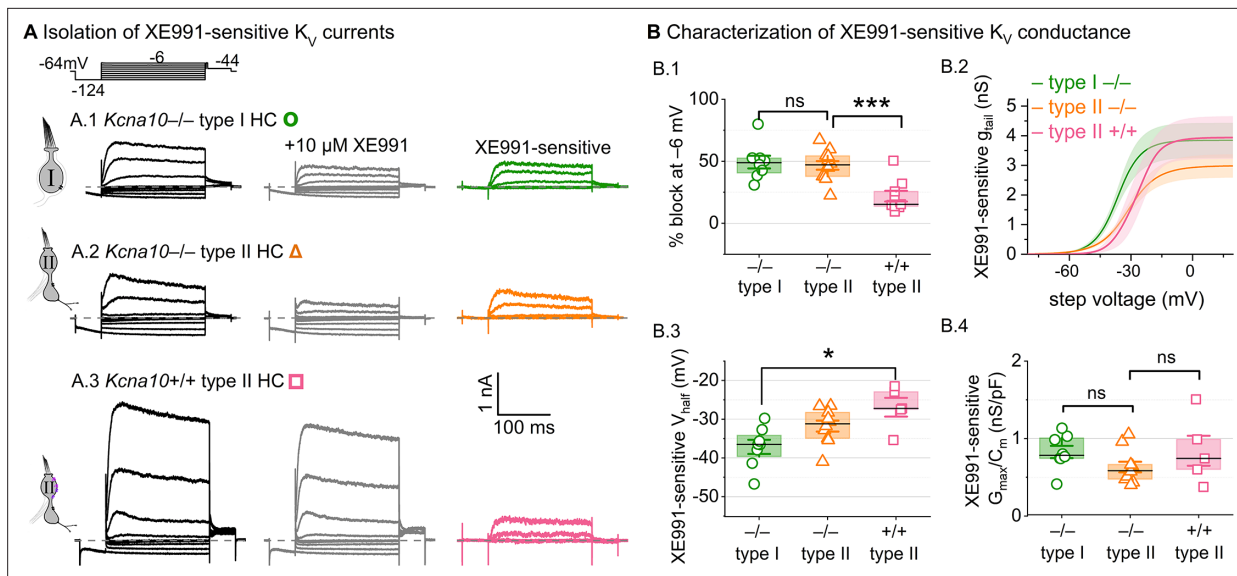
Figure 7. A K$_V$7-selective blocker, XE991, reduced residual delayed rectifier currents in *Kcna10$^{-/-}$* type I and II hair cells (HCs). (**A**) XE991 (10 μM) partly blocked similar delayed rectifier currents in type I and II *Kcna10$^{-/-}$* HCs and a type II *Kcna10$^{+/+}$* HC. (**B**) Properties of XE991-sensitive conductance, $_{DR}$(K$_V$7). (**B.1**) % Block of steady-state current. (**B.2**) Mean tail *G–V* curves for *Kcna10$^{-/-}$* type I HCs (n = 8), *Kcna10$^{-/-}$* type II HCs (9), and *Kcna10$^{+/+}$* type II HCs (5); shading is ± SEM. (**B.3**) V_{half} was less negative in *Kcna10$^{+/+}$* type II than *Kcna10$^{-/-}$* type I HC (p = 0.01, KWA). (**B.4**) Conductance density was similar in all groups (ANOVA), non-significant at 0.4 power (*left*), 0.2 power (*right*). *Asterisks*: *p < 0.05 and ***p < 0.001. *Line*, median; *Box*, interquartile range; *Whiskers*, outliers.

The online version of this article includes the following figure supplement(s) for figure 7:

Figure supplement 1. A minority of striolar *Kcna10$^{-/-}$* type I hair cells (HCs) had a small low-voltage-activated outward rectifier current in addition to a more positively activating outward rectifier.

Figure supplement 2. No difference was detected in H (HCN) and Kir (fast inward rectifier) currents between *Kcna10$^{+/+}$* and *Kcna10$^{-/-}$* hair cells (HCs), consistent with a specific involvement of K$_V$1.8 in *Kcna10* expression.

found them similar across genotypes (*Figure 7—figure supplement 2*). The $g_{K,L}$ knockout allowed identification of zonal differences in I_H and I_{Kir} in type I HCs, previously examined in type II HCs (*Masetto and Correia, 1997*; *Levin and Holt, 2012*). In type I HCs from both control and null utricles, I_H and I_{Kir} were less prevalent in striola than extrastriola, and, when present, the combined inward current was smaller (*Figure 7—figure supplement 2*).

Discussion

We have shown that constitutive knockout of K$_V$1.8 eliminated $g_{K,L}$ in type I HCs, and g_A and much of g_{DR} in type II HCs. K$_V$1.8 immunolocalized specifically to the basolateral membranes of type I and II HCs. We conclude that K$_V$1.8 is a pore-forming subunit of $g_{K,L}$, g_A, and part of g_{DR} [g_{DR}(K$_V$1.8)]. We suggest that fast inactivation of g_A may arise from heteromultimerization of non-inactivating K$_V$1.8 subunits and inactivating K$_V$1.4 subunits. Finally, we showed that a substantial component of the residual delayed rectifier current in both type I and II HCs comprises K$_V$7 channels.

K$_V$1.8 is expressed in HCs from mammalian cochlea (*Dierich et al., 2020*), avian utricle (*Scheibinger et al., 2022*), and zebrafish (*Erickson and Nicolson, 2015*). Our work suggests that in anamniotes, which lack type I cells and $g_{K,L}$, K$_V$1.8 contributes to g_A and g_{DR}, which are widespread in vertebrate HCs (reviewed in *Meredith and Rennie, 2016*). K$_V$1.8 expression has not been detected in rodent brain but is reported in the pacemaker nucleus of weakly electric fish (*Smith et al., 2018*).

K$_V$1.8 subunits may form homomultimers to produce $g_{K,L}$ in type I HCs

Recent single-cell expression studies on mouse utricles (*McInturff et al., 2018*; *Jan et al., 2021*; *Orvis et al., 2021*) have detected just one K$_V$1 subunit, K$_V$1.8, in mouse type I HCs. Given that K$_V$1.8 can only form multimers with K$_V$1 family members, and given that $g_{K,L}$ channels are present at very

high density (~150 per μm^2 in rat type I, **Chen and Eatock, 2000**), it stands to reason that most or all of the channels are K_V1.8 homomers. Other evidence is consistent with this proposal. $g_{K,L}$ (**Rüsch and Eatock, 1996a**) and heterologously expressed K_V1.8 homomers in oocytes (**Lang et al., 2000**) are non-inactivating and blocked by millimolar Ba^{2+} and 4-aminopyridine and >10 mM tetraethyl ammonium. Unlike channels with K_V1.1, K_V1.2, and K_V1.6 subunits, $g_{K,L}$ is not sensitive to 10 nM α-dendrotoxin (**Rüsch and Eatock, 1996a**). $g_{K,L}$ and heterologously expressed K_V1.8 channels have similar single-channel conductances (~20 pS for $g_{K,L}$ at positive potentials, **Chen and Eatock, 2000**; 11 pS in oocytes, **Lang et al., 2000**). $g_{K,L}$ is inhibited—or positively voltage-shifted—by cGMP (**Behrend et al., 1997**; **Chen and Eatock, 2000**), presumably via the C-terminal cyclic nucleotide-binding domain of K_V1.8.

A major novel property of $g_{K,L}$ is that it activates 30–60 mV negative to type II K_V1.8 conductances and most other low-voltage-activated K_V channels (**Ranjan et al., 2019**). The very negative activation range is a striking difference between $g_{K,L}$ and known homomeric K_V1.8 channels. Heterologously expressed homomeric K_V1.8 channels have an activation V_{half} of –10 to 0 mV (*X. laevis* oocytes, **Lang et al., 2000**; Chinese hamster ovary cells, **Dierich et al., 2020**). In cochlear inner HCs, currents attributed to K_V1.8 (by subtraction of other candidates) have a near-zero activation V_{half} (–4 mV, **Dierich et al., 2020**).

Possible factors in the unusually negative voltage dependence of $g_{K,L}$ include:

(1) *Elevation of extracellular K^+* by the enveloping calyceal terminal, unique to type I HCs (**Lim et al., 2011**; **Contini et al., 2012**; **Spaiardi et al., 2020**; **Govindaraju et al., 2023**). High K^+ increases conductance though $g_{K,L}$ channels (**Contini et al., 2020**), perhaps through K^+-mediated relief of C-type inactivation (**López-Barneo et al., 1993**; **Baukrowitz and Yellen, 1995**). We note, however, that $g_{K,L}$ is open at rest even in neonatal mouse utricles cultured without innervation (**Rüsch et al., 1998**) and persists in dissociated type I HCs (**Chen and Eatock, 2000**; **Hurley et al., 2006**).

(2) *The high density of $g_{K,L}$* (~50 nS/pF in striolar *Kcna10$^{+/+}$* HCs) implies close packing of channels, possibly represented by particles (12–14 nm) seen in freeze-fracture electron microscopy of the type I HC membrane (**Gulley and Bagger-Sjöbäck, 1979**; **Sousa et al., 2009**). Such close channel packing might hyperpolarize in situ voltage dependence of $g_{K,L}$, as proposed for K_V7.4 channels in outer HCs (**Perez-Flores et al., 2020**). Type I HC-specific partners that may facilitate this close packing include ADAM11 (**McInturff et al., 2018**), which clusters presynaptic K_V1.1 and K_V1.2 to enable ephaptic coupling at a cerebellar synapse (**Kole et al., 2015**).

(3) *Modulation by accessory subunits.* Type I HCs express K_Vβ1 (**McInturff et al., 2018**; **Orvis et al., 2021**), an accessory subunit that can confer fast inactivation and hyperpolarize activation V_{half} by ~10 mV. K_Vβ1 might interact with K_V1.8 to shift voltage dependence negatively. Arguments against this possibility include that $g_{K,L}$ lacks fast inactivation (**Rüsch and Eatock, 1996a**; **Hurley et al., 2006**; **Spaiardi et al., 2017**) and that cochlear inner HCs co-express K_V1.8 and K_Vβ1 (**Liu et al., 2018**) but their K_V1.8 conductance has a near-0 V_{half} (**Dierich et al., 2020**).

K_V1.8 subunits may combine with different subunits to produce g_A and K_V1.8-dependent g_{DR} in type II HCs

The K_V1.8-dependent conductances of type II HCs vary in their fast and slow inactivation. In not showing fast inactivation (**Lang et al., 2000**; **Ranjan et al., 2019**; **Dierich et al., 2020**), heterologously expressed K_V1.8 subunits resemble most other K_V1 family subunits, with the exception of K_V1.4 (for comprehensive review, see **Ranjan et al., 2019**). K_V1.4 is a good candidate to provide fast inactivation based on immunolocalization and voltage dependence (**Figures 4 and 6**). We suggest that g_A and $g_{DR}(K_V$1.8) are K_V1.8-containing channels that may include a variable number of K_V1.4 subunits and K_Vβ2 and K_Vβ1 accessory subunits.

K_V1.4–K_V1.8 heteromeric assembly could account for several related observations. The faster $\tau_{Inact,Fast}$ in *Kcna10$^{+/-}$* relative to *Kcna10$^{+/+}$* type II HCs (**Figure 3A.3**, **Figure 3—figure supplement 1A.1**) could reflect an increased ratio of K_V1.4–K_V1.8 subunits and therefore more N-terminal inactivation domains per heteromeric channel. Zonal variation in the extent and speed of N-type inactivation (**Figure 3A**) might arise from differential expression of K_V1.4. The small fast-inactivating conductance in ~20% of extrastriolar *Kcna10$^{-/-}$* type II HCs (**Figure 3—figure supplement 3**) might flow through K_V1.4 homomers.

Fast inactivation may also receive contribution from $K_V\beta$ subunits. $K_V\beta1$ is expressed in type II HCs (**McInturff et al., 2018**; **Jan et al., 2021**; **Orvis et al., 2021**), and, together with $K_V1.4$, has been linked to g_A in pigeon vestibular HCs (**Correia et al., 2008**). $K_V\beta2$, also expressed in type II HCs (**McInturff et al., 2018**; **Orvis et al., 2021**), accelerates but does not confer fast inactivation.

We speculate that g_A and $g_{DR}(K_V1.8)$ have different subunit composition: g_A may include heteromers of $K_V1.8$ with other subunits that confer rapid inactivation, while $g_{DR}(K_V1.8)$ may comprise homomeric $K_V1.8$ channels, given that they do not have N-type inactivation.

$K_V1.8$ relevance for vestibular function

In both type I and II utricular HCs, $K_V1.8$-dependent channels strongly shape receptor potentials in ways that promote temporal fidelity rather than electrical tuning (**Lewis, 1988**), consistent with the utricle's role in driving reflexes that compensate for head motions as they occur. This effect is especially pronounced for type I HCs, where the current-step evoked voltage response reproduces the input with great speed and linearity (**Figure 2**).

$g_{K,L}$ dominates passive membrane properties in mature $Kcna10^{+/+,+/-}$ type I HCs such that $Kcna10^{-/-}$ type I HCs are expected to have receptor potentials with higher amplitudes but lower low-pass corner frequencies, closer to those of type II HCs and immature HCs of all types (**Correia et al., 1996**; **Rüsch and Eatock, 1996a**; **Songer and Eatock, 2013**). In $Kcna10^{-/-}$ epithelia, we expect the lack of a large basolateral conductance open at rest to reduce the speed and gain of non-quantal transmission, which depends on K^+ ion efflux from the type I HC to change electrical and K^+ potentials in the synaptic cleft (**Govindaraju et al., 2023**). In HCs, K^+ enters the mechanosensitive channels of the hair bundle from the K^+-rich apical endolymph and exits through basolateral potassium conductances into the more conventional low-K^+ perilymph. For the type I-calyx synapse, having in the HC a large, non-inactivating K^+ conductance open across the physiological range of potentials avoids channel gating time and allows for instantaneous changes in current into the cleft and fast afferent signaling (**Pastras et al., 2023**).

In contrast, mature type II HCs face smaller synaptic contacts and have $K_V1.8$-dependent currents that are not substantially activated at resting potential. They do affect the time course and gain of type II HC responses to input currents, speeding up depolarizing transients, producing a repolarizing rebound during the step, and reducing resonance.

Type I and II vestibular HCs are closely related, such that adult type II HCs acquire type I-like properties upon deletion of the transcription factor *Sox2* (**Stone et al., 2021**). In normal development of the two cell types, the *Kcna10* gene generates biophysically distinct and functionally different ion channels, presenting a natural experiment in functional differentiation of sensory receptor cells.

Materials and methods

Key resources table

Reagent type (species) or resource	Designation	Source or reference	Identifiers	Additional information
Antibody	Anti-Kv1.8 (Rabbit polyclonal)	Alomone	Cat# APC-157, lot# 0102, RRID:AB_2341039	1:200 or 1:400
Antibody	Anti-calretinin (goat polyclonal)	Millipore	Cat# AB1550, lot# 9669, RRID:AB_90764	1:600
Antibody	Anti-Kv7.4 (mouse IgG1 monoclonal)	NeuroMab	Cat# 2HK-65, RRID:AB_2131828	1:200
Peptide, recombinant protein	Iberiotoxin	Alomone	STI-400	100 nM (water)
Chemical compound, drug	XE991	Sigma	X2254	100 µM (water)
Chemical compound, drug	ZD7288	Tocris	APN18035-2	100 µM (water)
Peptide, recombinant protein	Bovine serum albumin	Fisher	BP671	1 mg/ml (water)

Preparation

All procedures for handling animals followed the NIH Guide for the Care and Use of Laboratory Animals and were approved by the Institutional Animal Care and Use Committees of the University

of Chicago (Animal Care and Use Procedure #72360) and the Office of Animal Care and Institutional Biosafety at the University of Illinois Chicago (Protocol for Animal Use #17106). Most mice belonged to a transgenic line with a knockout allele of $Kcna10$ (referred to here as $Kcna10^{-/-}$). Our breeding colony was established with a generous gift of such animals from Sherry M. Jones and Thomas Friedman. These animals are described in their paper (*Lee et al., 2013*). Briefly, the Texas A&M Institute for Genomic Medicine generated the line on a C57BL/6;129SvEv mixed background by replacing Exon 3 of the $Kcna10$ gene with an IRES-bGeo/Purocassette. Mice in our colony were raised on a 12:12 hr light–dark cycle with access to food and water ad libitum.

Semi-intact utricles were prepared from ~150 male and ~120 female mice, postnatal days (P) 5–375, for same-day recording. HC K_V channel data were pooled across sexes as most results did not appear to differ by sex; an exception was that $g_{K,L}$ had a more negative V_{half} in males (*Supplementary file 1a*), an effect not clearly related to age, copy number, or other properties of the activation curve.

Preparation, stimulation, and recording methods followed our previously described methods for the mouse utricle (*Vollrath and Eatock, 2003*). Mice were anesthetized through isoflurane inhalation. After decapitation, each hemisphere was bathed in ice-cold, oxygenated Liebowitz-15 (L15) media. The temporal bone was removed, the labyrinth was cut to isolate the utricle, and the nerve was cut close to the utricle. The utricle was treated with proteinase XXIV (100 µg/ml, ~10 min, 22°C) to facilitate removal of the otoconia and attached gel layer and mounted beneath two glass rods affixed at one end to a coverslip.

Electrophysiology

We used the HEKA Multiclamp EPC10 with Patchmaster acquisition software, filtered by the integrated HEKA filters: a 6-pole Bessel filter at 10 kHz and a second 4-pole Bessel filter at 5 kHz, and sampled at 10–100 kHz. Recording electrodes were pulled (PC-100, Narishige) from soda lime glass (King's Precision Glass R-6) wrapped in paraffin to reduce pipette capacitance. Internal solution contained (in mM) 135 KCl, 0.5 $MgCl_2$, 3 MgATP, 5 4-(2-hydroxyethyl)piperazine-1-ethane-sulfonic acid (HEPES), 5 ethylene glycol tetraacetic acid (EGTA), 0.1 $CaCl_2$, 0.1 Na-cAMP, 0.1 LiGTP, 5 $Na_2CreatinePO_4$ adjusted to pH 7.25 and ~280 mmol/kg by adding ~30 mM KOH. External solution was Liebowitz-15 media supplemented with 10 mM HEPES (pH 7.40, 310 ± 10 mmol/kg). Recording temperature was 22–25°C. Pipette capacitance and membrane capacitance transients were subtracted during recordings with Patchmaster software. Series resistance (8–12 MΩ) was measured after rupture and compensated 60–80% with the amplifier, to final values of ~2 MΩ. Potentials are corrected for remaining (uncompensated) series resistance and liquid junction potential of ~+4 mV, calculated with LJPCalc software (*Marino et al., 2014*).

$Kcna10^{-/-}$ HCs appeared healthy in that cells had resting potentials negative to –50 mV, cells lasted a long time (20–30 min) in ruptured patch recordings, membranes were not fragile, and extensive blebbing was not seen. Type I HCs with $g_{K,L}$ were transiently hyperpolarized to ~–90 mV to close $g_{K,L}$ enough to increase R_{input} above 100 MΩ, as needed to estimate series resistance and cell capacitance. The average resting potential, V_{rest}, was –87 mV ±1 (41), similar to the calculated E_K of –86.1 mV, which is not surprising given the large K^+ conductance of these cells. V_{rest} is likely more positive in vivo, where lower endolymphatic Ca^{2+} increases standing inward current through MET channels.

Voltage protocols to characterize K_V currents differed slightly for type I and II HCs. In standard protocols, the cell is held at a voltage near resting potential (–74 mV in type I and –64 mV in type II), then jumped to –124 mV for 200 ms in type I HCs in order to fully deactivate $g_{K,L}$ and 50 ms in type II HCs in order to remove baseline inactivation of g_A. The subsequent iterated step depolarizations lasted 500 ms in type I HCs because $g_{K,L}$ activates slowly (*Wong et al., 2004*) and 200 ms in type II HCs, where K_V conductances activate faster. The 50 ms tail voltage was near the reversal potential of HCN channels (–44 mV in mouse utricular HCs, *Rüsch et al., 1998*) to avoid HCN current contamination.

$G–V$ (activation) parameters for control type I cells may be expected to vary across experiments on semi-intact (as here), organotypically cultured and denervated (*Rüsch et al., 1998*), or dissociated-cell preparations, reflecting variation in retention of the calyx (Discussion) and voltage step durations (*Wong et al., 2004*) which elevate K^+ concentration around the HC. Nevertheless, the values we obtained for type I and II HCs resemble values recorded elsewhere, including experiments in which extra care was taken to avoid extracellular K^+ accumulation (*Spaiardi et al., 2017*; *Spaiardi et al., 2020*). The effects of K^+ accumulation on $g_{K,L}$'s steady-state activation curves are

small because the operating range is centered on E and can be characterized with relatively small currents (*Figure 1A*).

Pharmacology

Drug-containing solutions were locally with BASI Bee Hive syringes at a final flow rate of 20 µl/min and a dead time of ~30 s. Global bath perfusion was paused during drug perfusion and recording, and only one cell was used per utricle. Aliquots of test agents in solution were prepared, stored at –20°C, and thawed and added to external solution on the recording day (see Key Resources Table).

Analysis

Data analysis was performed with software from OriginLab (Northampton, MA) and custom MATLAB scripts using MATLAB fitting algorithms.

Fitting voltage dependence and time course of conductances

G–V curves. Current was converted to conductance (*G*) by dividing by driving force (*V* – E_K; E_K calculated from solutions). For type I HCs, tail *G–V* curves were generated from current 1 ms after the end of the iterated voltage test step. For type II HCs, peak *G–V* curves were generated from peak current during the step and steady-state *G–V* curves were generated from current 1 ms before the end of a 200-ms step. We fit *G–V* curves to the first-order Boltzmann equation (*Equation 1*) using a custom MATLAB function (fitzmann.m, *Source code 2*).

$$G\left(V\right) = G_{min} + \frac{G_{max}}{1 + exp(\frac{V_{half} - V}{S})} \tag{1}$$

V_{half} is the midpoint, and *S* is the slope factor, inversely related to curve steepness near activation threshold.

Activation time course of type II HCs. We fit current traces using a custom MATLAB function (fitkin.m, *Source code 1*). For type II HCs lacking fast inactivation, outward current activation was fit with *Equation 2*.

$$I\left(t\right) = I_{SS} * \left(1 - exp(-\frac{t}{\tau_w})\right)^n + I_0 \tag{2}$$

I_{SS} is steady-state current; τ_w is activation time constant (referred to elsewhere as τ_{Act}); *n* is the state factor related to the number of closed states (typically constrained to 3); and I_o is baseline current.

To measure activation and inactivation time course of g_A, we used *Equation 3* to fit outward K$^+$ currents evoked by steps from –125 mV to above –50 mV (*Rothman and Manis, 2003*).

$$I\left(t\right) = I_{max} * \left(1 - exp(-\frac{t}{\tau_w})\right)^n * \left[1 - Z * \left(f * \left(1 - exp(-\frac{t}{\tau_{zf}})\right) + (1-f) * \left(1 - exp(-\frac{t}{\tau_{zs}})\right)\right)\right] + I_0 \tag{3}$$

Z is total steady-state inactivation (0 ≤ *Z* < 1 means incomplete inactivation, which allows the equation to fit non-inactivating delayed rectifier currents); *f* is the fraction of fast inactivation relative to total inactivation; I_{max} is maximal current; τ_{zf} (referred to elsewhere as $\tau_{Inact,Fast}$) and τ_{zs} are the fast and slow inactivation time constants. We chose to compare fit parameters at 30 ± 2 mV (91), where fast and slow inactivation were consistently separable and g_A was maximized. In most *Kcna10$^{-/-}$* and some striolar *Kcna10$^{+/+,+/-}$* cells, where fast inactivation was absent and adjusted R^2 did not improve on a single-exponential fit by >0.01, we constrained *f* in *Equation 3* to 0 to avoid overfitting.

For *Peak G–V* relations, peak conductance was taken from fitted curves (*Equations 2 and 3*). To construct '*Steady-state*' *G–V* relations, we used current at 200 ms, which was only 6 ± 1% (94) greater than steady-state estimated from fits to *Equation 3* (*Figure 3C, D*).

Percent inactivation was calculated at 30 mV with *Equation 4*:

$$\% Inactivation = \left(I_{Peak} - I_{SS}\right) / I_{Peak} \tag{4}$$

I_{Peak} is maximal current, and I_{SS} is current at the end of a 200-ms voltage step.

The electrical resonance of type II HCs was quantified by fitting voltage responses to current injection steps (*Songer and Eatock, 2013*). We fit *Equation 5*, a damped sinusoid, to the voltage trace from half-maximum of the initial depolarizing peak until the end of the current step.

$$V(t) = V_{ss} + V_p * exp(-\frac{t}{\tau_e}) * \sin\left(2\pi f_e - \theta\right) \tag{5}$$

V_{ss} is steady-state voltage; V_p is the voltage of the peak response; τ_e is the decay time constant; f_e is the fundamental frequency; and θ is the phase angle shift.

Quality factor, Q_e, was calculated with *Equation 6* (*Crawford and Fettiplace, 1981*).

$$Q_e = \left[\left(\pi f_e \tau_e\right)^2 + 0.25\right]^{1/2} \tag{6}$$

Statistics

We give means ± SEM for normally distributed data, and otherwise, median and range. Data normality was assessed with the Shapiro–Wilk test for $n < 50$ and the Kolmogorov–Smirnov test for $n > 50$. To assess homogeneity of variance we used Levene's test. With homogeneous variance, we used two-way ANOVA for genotype and zone with the post hoc Tukey's test. When variance was non-homogeneous, we used one-way Welch ANOVA with the posthoc Games–Howell test. For data that were not normally distributed, we used the non-parametric one-way Kruskal–Wallis ANOVA (KWA) with posthoc Dunn's test. Effect size is Hedge's g (g). For age dependence, we used partial correlation coefficients controlling for genotype and zone. Statistical groups may have different median ages, but all have overlapping age ranges. In figures, asterisks represent p-value ranges as follows: $*p < 0.05$; $**p < 0.01$; $***p < 0.001$; $****p < 0.0001$.

Immunohistochemistry

Mice were anesthetized with Nembutal (80 mg/kg), then perfused transcardially with 40 ml of physiological saline containing heparin (400 IU), followed by 2 ml/g body weight fixative (4% paraformaldehyde, 1% picric acid, and 5% sucrose in 0.1 M phosphate buffer at pH 7.4, sometimes with 1% acrolein). Vestibular epithelia were dissected in phosphate buffer, and tissues were cryoprotected in 30% sucrose-phosphate buffer overnight at 4°C. Otoconia were dissolved with Cal-Ex (Fisher Scientific) for 10 min. Frozen sections (35 μm) were cut with a sliding microtome. Immunohistochemistry was performed on free-floating sections. Tissues were first permeabilized with 4% Triton X-100 in phosphate-buffered saline (PBS) for 1 hr at room temperature, then incubated with 0.5% Triton X-100 in a blocking solution of 0.5% fish gelatin and 1% bovine serum albumin for 1 hr at room temperature. Sections were incubated with two to three primary antibodies for 72 hr at 4°C and with two to three secondary antibodies. Sections were rinsed with PBS between and after incubations and mounted on slides in Mowiol (Calbiochem).

Additional information

Funding

Author contributions

Hannah R Martin, Conceptualization, Data curation, Software, Formal analysis, Investigation, Visualization, Methodology, Writing - original draft, Project administration, Writing – review and editing; Anna Lysakowski, Funding acquisition, Investigation, Methodology, Project administration, Writing – review and editing; Ruth Anne Eatock, Conceptualization, Supervision, Funding acquisition, Validation, Visualization, Methodology, Writing - original draft, Project administration, Writing – review and editing

Author ORCIDs

Hannah R Martin http://orcid.org/0000-0003-2028-5798
Anna Lysakowski https://orcid.org/0000-0001-6259-0294
Ruth Anne Eatock https://orcid.org/0000-0001-7547-2051

Ethics

All procedures for handling animals followed the NIH Guide for the Care and Use of Laboratory Animals and were approved by the Institutional Animal Care and Use Committees of the University of Chicago (Animal Care and Use Procedure #72360) and the Office of Animal Care and Institutional Biosafety at the University of Illinois Chicago (Protocol for Animal Use #17106).

Peer review material

Reviewer #1 (Public review): https://doi.org/10.7554/eLife.94342.4.sa1
Reviewer #2 (Public review): https://doi.org/10.7554/eLife.94342.4.sa2
Reviewer #3 (Public review): https://doi.org/10.7554/eLife.94342.4.sa3
Author response https://doi.org/10.7554/eLife.94342.4.sa4

Additional files

Supplementary files

• Supplementary file 1. This file contains descriptive and comparative statistics on three additional analyses of the dataset. (**a**) Test of sex differences in hair cell K_V channel data. (**b**) We did not detect a genotype effect on soma size of type I hair cells (HCs). (**c**) I_{Kir} and I_H were greater in the extrastriola (ES) than striola (S), but did not vary by genotype.

• MDAR checklist

• Source code 1. Fitkin.m is a MATLAB function to fit the activation and inactivation kinetics of K_V currents to *Equations 2; 3*. Fitkin.m processed current–time traces and output parameters found in *Figure 3*, *Figure 3—figure supplement 1*, and *Table 3*.

• Source code 2. Fitzmann.m is a MATLAB function to fit the activation voltage dependence of K_V currents to *Equation 1*. Fitzmann.m processed *G–V* data points and output parameters found in *Figure 1*, *Figure 3*, *Figure 7*, *Figure 1—figure supplement 1*, *Figure 3—figure supplement 2*, *Table 1*, *Table 4*, and *Supplementary file 1a*.

Data availability

Data generated and analyzed in this study are available on Dryad (https://doi.org/10.5061/dryad.37pvmcvrw). Dryad hosts downloadable spreadsheets that are organized as follows: F1_sourcedata, numerical data for Figure 1; F1-fs1_sourcedata, numerical data for Figure 1-figure supplement 1;

F2_sourcedata, numerical data for Figure 2; F3_sourcedata, numerical data for Figure 3; F3-fs1_sourcedata, numerical data for Figure 3—figure supplement 1; F3-fs2_sourcedata, numerical data for Figure 3—figure supplement 2; F3-fs3_sourcedata, numerical data for Figure 3—figure supplement 3; F4_sourcedata, numerical data for Figure 4; F6_sourcedata, numerical data for Figure 6; F7_sourcedata, numerical data for Figure 7; F7-fs1_sourcedata, numerical data for Figure 7—figure supplement 1; F7-fs2_sourcedata, numerical data for Figure 7—figure supplement 2.

The following dataset was generated:

Author(s)	Year	Dataset title	Dataset URL	Database and Identifier
Martin HR, Lysakowski A, Eatock RA	2024	The potassium channel subunit Kv1.8 (Kcna10) is essential for the distinctive outwardly rectifying conductances of type I and II vestibular hair cells	https://doi.org/10.5061/dryad.37pvmcvrw	Dryad Digital Repository, 10.5061/dryad.37pvmcvrw

References

Alexander SPH, Mathie A, Peters JA, Veale EL, Striessnig J, Kelly E, Armstrong JF, Faccenda E, Harding SD, Pawson AJ, Sharman JL, Southan C, Davies JA, CGTP Collaborators. 2019. The concise guide to pharmacology 2019/20: ion channels. *British Journal of Pharmacology* **176 Suppl 1**:S142–S228. DOI: https://doi.org/10.1111/bph.14749, PMID: 31710715

Al Sabi A, Kaza S, Le Berre M, O'Hara L, Bodeker M, Wang J, Dolly JO. 2011. Position-dependent attenuation by Kv1.6 of N-type inactivation of Kv1.4-containing channels. *The Biochemical Journal* **438**:389–396. DOI: https://doi.org/10.1042/BJ20102169, PMID: 21352098

Ashmore JF. 1983. Frequency tuning in a frog vestibular organ. *Nature* **304**:536–538. DOI: https://doi.org/10.1038/304536a0, PMID: 6603578

Bao H, Wong WH, Goldberg JM, Eatock RA. 2003. Voltage-gated calcium channel currents in type I and type II hair cells isolated from the rat crista. *Journal of Neurophysiology* **90**:155–164. DOI: https://doi.org/10.1152/jn.00244.2003, PMID: 12843307

Baukrowitz T, Yellen G. 1995. Modulation of K+ current by frequency and external [K+]: A tale of two inactivation mechanisms. *Neuron* **15**:951–960. DOI: https://doi.org/10.1016/0896-6273(95)90185-x, PMID: 7576643

Behrend O, Schwark C, Kunihiro T, Strupp M. 1997. Cyclic GMP inhibits and shifts the activation curve of the delayed-rectifier (I[K1]) of type I mammalian vestibular hair cells. *Neuroreport* **8**:2687–2690. DOI: https://doi.org/10.1097/00001756-199708180-00010, PMID: 9295101

Brown DA, Selyanko AA, Hadley JK, Tatulian L. 2002. Some pharmacological properties of neural KCNQ channels. *Neurophysiology* **34**:91–94. DOI: https://doi.org/10.1023/A:1020768914645

Carlisle FA, Steel KP, Lewis MA. 2012. Specific expression of *Kcna10, Pxn* and *Odf2* in the organ of Corti. *Gene Expression Patterns* **12**:172–179. DOI: https://doi.org/10.1016/j.gep.2012.03.001, PMID: 22446089

Chen JWY, Eatock RA. 2000. Major potassium conductance in Type I hair cells from rat semicircular canals: Characterization and modulation by nitric oxide. *Journal of Neurophysiology* **84**:139–151. DOI: https://doi.org/10.1152/jn.2000.84.1.139

Contini D, Zampini V, Tavazzani E, Magistretti J, Russo G, Prigioni I, Masetto S. 2012. Intercellular K+ accumulation depolarizes type I vestibular hair cells and their associated afferent nerve calyx. *Neuroscience* **227**:232–246. DOI: https://doi.org/10.1016/j.neuroscience.2012.09.051

Contini D, Price SD, Art JJ. 2017. Accumulation of K+ in the synaptic cleft modulates activity by influencing both vestibular hair cell and calyx afferent in the turtle: K+ modulation of synaptic transmission between hair cell and afferent. *J Physiol* **595**:777–803. DOI: https://doi.org/10.1113/JP273060

Contini D, Holstein GR, Art JJ. 2020. Synaptic cleft microenvironment influences potassium permeation and synaptic transmission in hair cells surrounded by calyx afferents in the turtle. *The Journal of Physiology* **598**:853–889. DOI: https://doi.org/10.1113/JP278680, PMID: 31623011

Correia MJ, Lang DG. 1990. An electrophysiological comparison of solitary type I and type II vestibular hair cells. *Neuroscience Letters* **116**:106–111. DOI: https://doi.org/10.1016/0304-3940(90)90394-O

Correia MJ, Ricci AJ, Rennie KJ. 1996. Filtering properties of vestibular hair cells: an update. *Annals of the New York Academy of Sciences* **781**:138–149. DOI: https://doi.org/10.1111/j.1749-6632.1996.tb15698.x

Correia MJ, Weng T, Prusak D, Wood TG. 2008. Kvβ1.1 associates with Kvα1.4 in Chinese hamster ovary cells and pigeon type II vestibular hair cells and enhances the amplitude, inactivation and negatively shifts the steady-state inactivation range. *Neuroscience* **152**:809–820. DOI: https://doi.org/10.1016/j.neuroscience.2008.01.021, PMID: 18313857

Crawford AC, Fettiplace R. 1981. An electrical tuning mechanism in turtle cochlear hair cells. *The Journal of Physiology* **312**:377–412. DOI: https://doi.org/10.1113/jphysiol.1981.sp013634, PMID: 7265000

Desai SS, Zeh C, Lysakowski A. 2005. Comparative morphology of rodent vestibular periphery. I. Saccular and utricular maculae. *Journal of Neurophysiology* **93**:251–266. DOI: https://doi.org/10.1152/jn.00746.2003, PMID: 15240767

Dierich M, Altoè A, Koppelmann J, Evers S, Renigunta V, Schäfer MK, Naumann R, Verhulst S, Oliver D, Leitner MG. 2020. Optimized tuning of auditory inner hair cells to encode complex sound through synergistic activity of six independent K$^+$ current entities. *Cell Reports* **32**:107869. DOI: https://doi.org/10.1016/j.celrep.2020.107869, PMID: 32640234

Dwenger MM, Raph SM, Baba SP, Moore JB, Nystoriak MA. 2022. Diversification of potassium currents in excitable cells via Kvβ proteins. *Cells* **11**:2230. DOI: https://doi.org/10.3390/cells11142230, PMID: 35883673

Eatock RA, Songer JE. 2011. Vestibular hair cells and afferents: two channels for head motion signals. *Annual Review of Neuroscience* **34**:501–534. DOI: https://doi.org/10.1146/annurev-neuro-061010-113710, PMID: 21469959

Erickson T, Nicolson T. 2015. Identification of sensory hair-cell transcripts by thiouracil-tagging in zebrafish. *BMC Genomics* **16**:842. DOI: https://doi.org/10.1186/s12864-015-2072-5, PMID: 26494580

Fettiplace R. 1987. Electrical tuning of hair cells in the inner ear. *Trends in Neurosciences* **10**:421–425. DOI: https://doi.org/10.1016/0166-2236(87)90013-0

Géléoc GSG, Risner JR, Holt JR. 2004. Developmental acquisition of voltage-dependent conductances and sensory signaling in hair cells of the embryonic mouse inner ear. *The Journal of Neuroscience* **24**:11148–11159. DOI: https://doi.org/10.1523/JNEUROSCI.2662-04.2004, PMID: 15590931

Goldberg JM. 2000. Afferent diversity and the organization of central vestibular pathways. *Experimental Brain Research* **130**:277–297. DOI: https://doi.org/10.1007/s002210050033, PMID: 10706428

González-Garrido A, Pujol R, López-Ramírez O, Finkbeiner C, Eatock RA, Stone JS. 2021. The differentiation status of hair cells that regenerate naturally in the vestibular inner ear of the adult mouse. *The Journal of Neuroscience* **41**:7779–7796. DOI: https://doi.org/10.1523/JNEUROSCI.3127-20.2021, PMID: 34301830

Govindaraju AC, Quraishi IH, Lysakowski A, Eatock RA, Raphael RM. 2023. Nonquantal transmission at the vestibular hair cell–calyx synapse: K$_{LV}$ currents modulate fast electrical and slow K$^+$ potentials. *PNAS* **120**:e2207466120. DOI: https://doi.org/10.1073/pnas.2207466120

Gulley RL, Bagger-Sjöbäck D. 1979. Freeze-fracture studies on the synapse between the type I hair cell and the calyceal terminal in the guinea-pig vestibular system. *Journal of Neurocytology* **8**:591–603. DOI: https://doi.org/10.1007/BF01208511, PMID: 317909

Holt JR, Vollrath MA, Eatock RA. 1999. Stimulus processing by type II hair cells in the mouse utricle. *Annals of the New York Academy of Sciences* **871**:15–26. DOI: https://doi.org/10.1111/j.1749-6632.1999.tb09172.x

Holt JR, Stauffer EA, Abraham D, Géléoc GSG. 2007. Dominant-negative inhibition of M-like potassium conductances in hair cells of the mouse inner ear. *The Journal of Neuroscience* **27**:8940–8951. DOI: https://doi.org/10.1523/JNEUROSCI.2085-07.2007, PMID: 17699675

Horwitz GC, Risner-Janiczek JR, Jones SM, Holt JR. 2011. HCN channels expressed in the inner ear are necessary for normal balance function. *The Journal of Neuroscience* **31**:16814–16825. DOI: https://doi.org/10.1523/JNEUROSCI.3064-11.2011, PMID: 22090507

Hudspeth AJ, Lewis RS. 1988. A model for electrical resonance and frequency tuning in saccular hair cells of the bull-frog, *Rana catesbeiana*. *The Journal of Physiology* **400**:275–297. DOI: https://doi.org/10.1113/jphysiol.1988.sp017120, PMID: 2458455

Hurley KM, Gaboyard S, Zhong M, Price SD, Wooltorton JRA, Lysakowski A, Eatock RA. 2006. M-like K+ currents in type I hair cells and calyx afferent endings of the developing rat utricle. *The Journal of Neuroscience* **26**:10253–10269. DOI: https://doi.org/10.1523/JNEUROSCI.2596-06.2006, PMID: 17021181

Imbrici P, D'Adamo MC, Kullmann DM, Pessia M. 2006. Episodic ataxia type 1 mutations in the *KCNA1* gene impair the fast inactivation properties of the human potassium channels Kv1.4-1.1/Kvβ1.1 and Kv1.4-1.1/Kvβ1.2. *The European Journal of Neuroscience* **24**:3073–3083. DOI: https://doi.org/10.1111/j.1460-9568.2006.05186.x, PMID: 17156368

Jan TA, Eltawil Y, Ling AH, Chen L, Ellwanger DC, Heller S, Cheng AG. 2021. Spatiotemporal dynamics of inner ear sensory and non-sensory cells revealed by single-cell transcriptomics. *Cell Reports* **36**:109358. DOI: https://doi.org/10.1016/j.celrep.2021.109358, PMID: 34260939

Jensen HS, Grunnet M, Olesen SP. 2007. Inactivation as a new regulatory mechanism for neuronal Kv7 channels. *Biophysical Journal* **92**:2747–2756. DOI: https://doi.org/10.1529/biophysj.106.101287, PMID: 17237198

Kharkovets T, Hardelin JP, Safieddine S, Schweizer M, El-Amraoui A, Petit C, Jentsch TJ. 2000. KCNQ4, a K+ channel mutated in a form of dominant deafness, is expressed in the inner ear and the central auditory pathway. *PNAS* **97**:4333–4338. DOI: https://doi.org/10.1073/pnas.97.8.4333, PMID: 10760300

Kole MJ, Qian J, Waase MP, Klassen TL, Chen TT, Augustine GJ, Noebels JL. 2015. Selective loss of presynaptic potassium channel clusters at the cerebellar basket cell terminal pinceau in *Adam11* mutants reveals their role in ephaptic control of purkinje cell firing. *The Journal of Neuroscience* **35**:11433–11444. DOI: https://doi.org/10.1523/JNEUROSCI.1346-15.2015, PMID: 26269648

Kubisch C, Schroeder BC, Friedrich T, Lütjohann B, El-Amraoui A, Marlin S, Petit C, Jentsch TJ. 1999. KCNQ4, a novel potassium channel expressed in sensory outer hair cells, is mutated in dominant deafness. *Cell* **96**:437–446. DOI: https://doi.org/10.1016/s0092-8674(00)80556-5, PMID: 10025409

Lang R, Lee G, Liu W, Tian S, Rafi H, Orias M, Segal AS, Desir GV. 2000. KCNA10: A novel ion channel functionally related to both voltage-gated potassium and CNG cation channels. *American Journal of Physiology-Renal Physiology* **278**:F1013–F1021. DOI: https://doi.org/10.1152/ajprenal.2000.278.6.F1013

Lee SI, Conrad T, Jones SM, Lagziel A, Starost MF, Belyantseva IA, Friedman TB, Morell RJ. 2013. A null mutation of mouse *Kcna10* causes significant vestibular and mild hearing dysfunction. *Hearing Research* **300**:1–9. DOI: https://doi.org/10.1016/j.heares.2013.02.009, PMID: 23528307

Levin ME, Holt JR. 2012. The function and molecular identity of inward rectifier channels in vestibular hair cells of the mouse inner ear. *Journal of Neurophysiology* **108**:175–186. DOI: https://doi.org/10.1152/jn.00098.2012, PMID: 22496522

Lewis ER. 1988. Tuning in the bullfrog ear. *Biophysical Journal* **53**:441–447. DOI: https://doi.org/10.1016/S0006-3495(88)83120-5, PMID: 3258166

Lim R, Kindig AE, Donne SW, Callister RJ, Brichta AM. 2011. Potassium accumulation between type I hair cells and calyx terminals in mouse crista. *Experimental Brain Research* **210**:607–621. DOI: https://doi.org/10.1007/s00221-011-2592-4

Liu H, Chen L, Giffen KP, Stringham ST, Li Y, Judge PD, Beisel KW, He DZZ. 2018. Cell-specific transcriptome analysis shows that adult pillar and deiters' cells express genes encoding machinery for specializations of cochlear hair cells. *Frontiers in Molecular Neuroscience* **11**:356. DOI: https://doi.org/10.3389/fnmol.2018.00356, PMID: 30327589

López-Barneo J, Hoshi T, Heinemann SH, Aldrich RW. 1993. Effects of external cations and mutations in the pore region on C-type inactivation of Shaker potassium channels. *Receptors & Channels* **1**:61–71 PMID: 8081712.

Lysakowski A, Goldberg JM. 2004. Morphophysiology of the vestibular periphery. Highstein SM, Fay RR, Popper AN (Eds). *The Vestibular System.* New York: Springer. p. 57–152. DOI: https://doi.org/10.1007/0-387-21567-0_3

Lysakowski A, Gaboyard-Niay S, Calin-Jageman I, Chatlani S, Price SD, Eatock RA. 2011. Molecular microdomains in a sensory terminal, the vestibular calyx ending. *The Journal of Neuroscience* **31**:10101–10114. DOI: https://doi.org/10.1523/JNEUROSCI.0521-11.2011, PMID: 21734302

Marino M, Misuri L, Brogioli D. 2014. A new open source software for the calculation of the liquid junction potential between two solutions according to the stationary nernst-planck equation. [arXiv]. http://arxiv.org/abs/1403.3640

Masetto S, Correia MJ. 1997. Electrophysiological properties of vestibular sensory and supporting cells in the labyrinth slice before and during regeneration. *Journal of Neurophysiology* **78**:1913–1927. DOI: https://doi.org/10.1152/jn.1997.78.4.1913

McInturff S, Burns JC, Kelley MW. 2018. Characterization of spatial and temporal development of Type I and Type II hair cells in the mouse utricle using new cell-type-specific markers. *Biology Open* **7**:bio038083. DOI: https://doi.org/10.1242/bio.038083, PMID: 30455179

Meredith FL, Rennie KJ. 2016. Channeling your inner ear potassium: K+ channels in vestibular hair cells. *Hearing Research* **338**:40–51. DOI: https://doi.org/10.1016/j.heares.2016.01.015

Mitra K, Ubarretxena-Belandia I, Taguchi T, Warren G, Engelman DM. 2004. Modulation of the bilayer thickness of exocytic pathway membranes by membrane proteins rather than cholesterol. *PNAS* **101**:4083–4088. DOI: https://doi.org/10.1073/pnas.0307332101, PMID: 15016920

Orvis J, Gottfried B, Kancherla J, Adkins RS, Song Y, Dror AA, Olley D, Rose K, Chrysostomou E, Kelly MC, Milon B, Matern MS, Azaiez H, Herb B, Colantuoni C, Carter RL, Ament SA, Kelley MW, White O, Bravo HC, et al. 2021. gEAR: gene expression analysis resource portal for community-driven, multi-omic data exploration. *Nature Methods* **18**:843–844. DOI: https://doi.org/10.1038/s41592-021-01200-9, PMID: 34172972

Pastras CJ, Curthoys IS, Asadnia M, McAlpine D, Rabbitt RD, Brown DJ. 2023. Evidence that ultrafast nonquantal transmission underlies synchronized vestibular action potential generation. *The Journal of Neuroscience* **43**:7149–7157. DOI: https://doi.org/10.1523/JNEUROSCI.1417-23.2023, PMID: 37775302

Perez-Flores MC, Lee JH, Park S, Zhang XD, Sihn CR, Ledford HA, Wang W, Kim HJ, Timofeyev V, Yarov-Yarovoy V, Chiamvimonvat N, Rabbitt RD, Yamoah EN. 2020. Cooperativity of K_V7.4 channels confers ultrafast electromechanical sensitivity and emergent properties in cochlear outer hair cells. *Science Advances* **6**:eaba1104. DOI: https://doi.org/10.1126/sciadv.aba1104, PMID: 32285007

Pujol R, Pickett SB, Nguyen TB, Stone JS. 2014. Large basolateral processes on type II hair cells are novel processing units in mammalian vestibular organs. *The Journal of Comparative Neurology* **522**:3141–3159. DOI: https://doi.org/10.1002/cne.23625, PMID: 24825750

Ramanathan K, Fuchs PA. 2002. Modeling hair cell tuning by expression gradients of potassium channel beta subunits. *Biophysical Journal* **82**:64–75. DOI: https://doi.org/10.1016/S0006-3495(02)75374-5, PMID: 11751296

Ranjan R, Logette E, Marani M, Herzog M, Tâche V, Scantamburlo E, Buchillier V, Markram H. 2019. A kinetic map of the homomeric voltage-gated potassium channel (Kv) family. *Frontiers in Cellular Neuroscience* **13**:358. DOI: https://doi.org/10.3389/fncel.2019.00358, PMID: 31481875

Rennie KJ, Correia MJ. 1994. Potassium currents in mammalian and avian isolated type I semicircular canal hair cells. *Journal of Neurophysiology* **71**:317–329. DOI: https://doi.org/10.1152/jn.1994.71.1.317

Rennie KJ, Weng T, Correia MJ. 2001. Effects of KCNQ channel blockers on K+ currents in vestibular hair cells . *American Journal of Physiology-Cell Physiology* **280**:C473–C480. DOI: https://doi.org/10.1152/ajpcell.2001.280.3.C473

Ricci AJ, Rennie KJ, Correia MJ. 1996. The delayed rectifier, I_{KI}, is the major conductance in type I vestibular hair cells across vestibular end organs. *Pflügers Archiv - European Journal of Physiology* **432**:34–42. DOI: https://doi.org/10.1007/s004240050102

Rothman JS, Manis PB. 2003. Kinetic analyses of three distinct potassium conductances in ventral cochlear nucleus neurons. *Journal of Neurophysiology* **89**:3083–3096. DOI: https://doi.org/10.1152/jn.00126.2002

Rüsch A, Eatock RA. 1996a. A delayed rectifier conductance in type I hair cells of the mouse utricle. *Journal of Neurophysiology* **76**:995–1004. DOI: https://doi.org/10.1152/jn.1996.76.2.995, PMID: 8871214

Rüsch A, Eatock RA. 1996b. Voltage responses of mouse utricular hair cells to injected currents. *Annals of the New York Academy of Sciences* **781**:71–84. DOI: https://doi.org/10.1111/j.1749-6632.1996.tb15694.x, PMID: 8694485

Rüsch A, Lysakowski A, Eatock RA. 1998. Postnatal development of type I and type II hair cells in the mouse utricle: acquisition of voltage-gated conductances and differentiated morphology. *The Journal of Neuroscience* **18**:7487–7501. DOI: https://doi.org/10.1523/JNEUROSCI.18-18-07487.1998, PMID: 9736667

Scheffer DI, Shen J, Corey DP, Chen ZY. 2015. Gene expression by mouse inner ear hair cells during development. *The Journal of Neuroscience* **35**:6366–6380. DOI: https://doi.org/10.1523/JNEUROSCI.5126-14.2015, PMID: 25904789

Scheibinger M, Janesick A, Benkafadar N, Ellwanger DC, Jan TA, Heller S. 2022. Cell-type identity of the avian utricle. *Cell Reports* **40**:111432. DOI: https://doi.org/10.1016/j.celrep.2022.111432, PMID: 36170825

Schroeder BC, Hechenberger M, Weinreich F, Kubisch C, Jentsch TJ. 2000. KCNQ5, a novel potassium channel broadly expressed in brain, mediates M-type currents. *Journal of Biological Chemistry* **275**:24089–24095. DOI: https://doi.org/10.1074/jbc.M003245200

Schweizer FE, Savin D, Luu C, Sultemeier DR, Hoffman LF. 2009. Distribution of high-conductance calcium-activated potassium channels in rat vestibular epithelia. *The Journal of Comparative Neurology* **517**:134–145. DOI: https://doi.org/10.1002/cne.22148, PMID: 19731297

Smith GT, Proffitt MR, Smith AR, Rusch DB. 2018. Genes linked to species diversity in a sexually dimorphic communication signal in electric fish. *Journal of Comparative Physiology. A, Neuroethology, Sensory, Neural, and Behavioral Physiology* **204**:93–112. DOI: https://doi.org/10.1007/s00359-017-1223-3, PMID: 29058069

Songer JE, Eatock RA. 2013. Tuning and timing in mammalian type I hair cells and calyceal synapses. *The Journal of Neuroscience* **33**:3706–3724. DOI: https://doi.org/10.1523/JNEUROSCI.4067-12.2013, PMID: 23426697

Sousa AD, Andrade LR, Salles FT, Pillai AM, Buttermore ED, Bhat MA, Kachar B. 2009. The septate junction protein Caspr is required for structural support and retention of KCNQ4 at calyceal synapses of vestibular hair cells. *The Journal of Neuroscience* **29**:3103–3108. DOI: https://doi.org/10.1523/JNEUROSCI.4868-08.2009, PMID: 19279247

Spaiardi P, Tavazzani E, Manca M, Milesi V, Russo G, Prigioni I, Marcotti W, Magistretti J, Masetto S. 2017. An allosteric gating model recapitulates the biophysical properties of $I_{K,L}$ expressed in mouse vestibular type I hair cells. *The Journal of Physiology* **595**:6735–6750. DOI: https://doi.org/10.1113/JP274202, PMID: 28862328

Spaiardi P, Tavazzani E, Manca M, Russo G, Prigioni I, Biella G, Giunta R, Johnson SL, Marcotti W, Masetto S. 2020. K^+ accumulation and clearance in the calyx synaptic cleft of type I mouse vestibular hair cells. *Neuroscience* **426**:69–86. DOI: https://doi.org/10.1016/j.neuroscience.2019.11.028, PMID: 31846752

Spitzmaul G, Tolosa L, Winkelman BHJ, Heidenreich M, Frens MA, Chabbert C, Zeeuw CI, Jentsch TJ. 2013. Vestibular role of KCNQ4 and KCNQ5 K^+ channels revealed by mouse models. *Journal of Biological Chemistry* **288**:9334–9344. DOI: https://doi.org/10.1074/jbc.M112.433383

Stone JS, Pujol R, Nguyen TB, Cox BC. 2021. The transcription factor sox2 is required to maintain the cell type-specific properties and innervation of type II vestibular hair cells in adult mice. *The Journal of Neuroscience* **41**:6217–6233. DOI: https://doi.org/10.1523/JNEUROSCI.1831-20.2021, PMID: 34099510

Stühmer W, Ruppersberg JP, Schröter KH, Sakmann B, Stocker M, Giese KP, Perschke A, Baumann A, Pongs O. 1989. Molecular basis of functional diversity of voltage-gated potassium channels in mammalian brain. *The EMBO Journal* **8**:3235–3244. DOI: https://doi.org/10.1002/j.1460-2075.1989.tb08483.x, PMID: 2555158

Vollrath MA, Eatock RA. 2003. Time course and extent of mechanotransducer adaptation in mouse utricular hair cells: comparison with frog saccular hair cells. *Journal of Neurophysiology* **90**:2676–2689. DOI: https://doi.org/10.1152/jn.00893.2002

Wang H. 1998. KCNQ2 and KCNQ3 potassium channel subunits: molecular correlates of the M-channel. *Science* **282**:1890–1893. DOI: https://doi.org/10.1126/science.282.5395.1890

Weng T, Correia MJ. 1999. Regional distribution of ionic currents and membrane voltage responses of type II hair cells in the vestibular neuroepithelium. *Journal of Neurophysiology* **82**:2451–2461. DOI: https://doi.org/10.1152/jn.1999.82.5.2451, PMID: 10561418

Wersall J. 1956. Studies on the structure and innervation of the sensory epithelium of the cristae ampulares in the guinea pig; a light and electron microscopic investigation. *Acta Oto-Laryngologica. Supplementum* **126**:1–85 PMID: 13326368.

Wong WH, Hurley KM, Eatock RA. 2004. Differences between the negatively activating potassium conductances of mammalian cochlear and vestibular hair cells. *Journal of the Association for Research in Otolaryngology* **5**:270–284. DOI: https://doi.org/10.1007/s10162-004-4051-4, PMID: 15492886

Xu T, Nie L, Zhang Y, Mo J, Feng W, Wei D, Petrov E, Calisto LE, Kachar B, Beisel KW, Vazquez AE, Yamoah EN. 2007. Roles of alternative splicing in the functional properties of inner ear-specific KCNQ4 channels. *Journal of Biological Chemistry* **282**:23899–23909. DOI: https://doi.org/10.1074/jbc.M702108200

Yao X, Tian S, Chan H-Y, Biemesderfer D, Desir GV. 2002. Expression of KCNA10, a voltage-gated K channel, in glomerular endothelium and at the apical membrane of the renal proximal tubule. *Journal of the American Society of Nephrology* **13**:2831–2839. DOI: https://doi.org/10.1097/01.ASN.0000036866.37886.C5